

Spatio-temporal variability of zooplankton standing stock in
eastern Arabian Sea inferred from ADCP backscatter
measurements

Ranjan Kumar Sahu, P. Amol, D.V. Desai, S.G. Aparna, D. Shankar

September 13, 2024

Abstract

We use acoustic Doppler current profiler (ADCP) backscatter measurements to map the spatio-temporal variation of zooplankton standing stock in the eastern Arabian Sea (EAS). The ADCP moorings were deployed at seven locations on the continental slope off the west coast of India; we use data from October 2017 to December 2023. The 153.3 kHz ADCP uses backscatter from sediments or organisms such as copepods, ctenophores, salps and amphipods greater than 1 cm to calculate current profile. The backscatter is obtained from echo intensity using RSSI conversion factor after doing necessary calibrations. The conversion from backscatter to biomass is based on volumetric zooplankton sampling at the respective locations. Analysis of the data over 24 – 120 m shows that the backscatter and zooplankton biomass decrease from the upper ocean (215 m g^{-3} biomass contour) to the lower depths. Changes are observed in the seasonal variation of the monthly

¹² climatology of zooplankton standing stock (integral of the biomass over 24 – 120 m water column)
¹³ as we move to poleward along the slope in EAS. The range of variation of standing stock is lowest
¹⁴ at Kanyakumari, followed by Okha, which lie at the southern and northern boundary of the EAS,
¹⁵ respectively. Complementary variables are used to explain the processes leading to growth or decay
¹⁶ of zooplankton biomass.

₁₇ **1 Introduction**

₁₈ **1.1 Background**

₁₉ Zooplankton plays a vital role in food web of pelagic ecosystem by enabling the hierarchical trans-
₂₀ port of organic matter from primary producers to higher trophic levels impacting the fish population
₂₁ and the carbon pump of the deep ocean [Ohman and Hirche, 2001, Le Qu et al., 2016]. They are
₂₂ presumably the largest migrating organisms in terms of biomass [Hays, 2003] which occurs in diel
₂₃ vertical migration (DVM). Zooplanktons depend not only on phytoplankton but other environ-
₂₄ mental parameters (e.g. Mixed layer depth, insolation, Oxygen, thermocline, nutrient availability,
₂₅ chlorophyll concentration and daily primary production). The biological productivity of the ocean
₂₆ is essentially connected with physics and chemistry [Subrahmanyam, 1959, Ryther et al., 1966,
₂₇ Qasim, 1977, Nair, 1970, Banse, 1995, McCreary et al., 2009, Vijith et al., 2016, Amol et al., 2020].
₂₈ The dynamic ocean results in varying physico-chemical properties, leading to bloom and growth
₂₉ of planktons in favourable conditions. The changes are strongly influenced by the seasonal cycle
₃₀ in the North Indian Ocean (NIO; north of 5 °N of Indian Ocean). The eastern boundary of Ara-
₃₁ bian Sea contains the West India Coastal Current (WICC; [Patil et al., 1964, Ramamirtham and
₃₂ Murty, 1965, Banse, 1968, Shetye et al., 1991, McCreary Jr et al., 1993, Shankar and Shetye, 1997,
₃₃ Shetye and Gouveia, 1998, Maheswaran et al., 2000, Schott and McCreary, 2001, Amol et al., 2014,
₃₄ Chaudhuri et al., 2020, 2021]) which reverses seasonally, flowing poleward (equatorward) during
₃₅ November to February (June to September).

₃₆ The direct consequence of this reversal is the seasonal cycle of thermocline, oxycline and thick-
₃₇ ness of mixed Layer Depth (MLD) induced by upwelling favourable conditions in summer and down-
₃₈ welling favourable conditions in winter in eastern Arabian Sea (EAS). Further, the phytoplankton

39 biomass and chlorophyll concentration changes with the season [Subrahmanyam and Sarma, 1960,
40 Banse, 1968, Lévy et al., 2007, Vijith et al., 2016]. Upwelling in summer monsoon leads to maximum
41 chlorophyll growth in the entire EAS [Banse, 1968, Banse and English, 2000, McCreary et al., 2009,
42 Hood et al., 2017, Shi and Wang, 2022]. During winter monsoon, the convective mixing induced
43 winter mixed layer [Shetye et al., 1992, Madhupratap et al., 1996b, Lévy et al., 2007, Vijith et al.,
44 2016, Shankar et al., 2016, Keerthi et al., 2017, Shi and Wang, 2022] results in winter chlorophyll
45 peak in northern EAS (NEAS) while the downwelling Rossby waves modulate chlorophyll along the
46 southern EAS (SEAS) albeit limited to coast and islands [Amol et al., 2020].

47 The zooplankton grazing peak is instantaneous with no time delay from peak phytoplankton
48 production [Li et al., 2000, Barber et al., 2001], but its population growth lags [Rehim and Imran,
49 2012, Almén and Tamelander, 2020] depending on its gestation period and other limiting aspects.
50 While some studies suggest that the peak timing of zooplankton may not change in parallel with
51 phytoplankton blooms [Winder and Schindler, 2004], others indicate that lag exists between primary
52 production and the transfer of energy to higher trophic levels [Brock and McClain, 1992, Brock et al.,
53 1991]. In their work, Aparna et al. [2022] (A22 from hereon) had shown that peak zooplankton
54 population may never occur even with a bloom in phytoplankton such as in SEAS, leading to the
55 collapse of ecological models and succeeding food webs of higher trophic levels.

56 The conventional zooplankton measurements, where only few snapshot/s of the event is captured
57 gives an incoherent or incomplete understanding in terms of spatio-temporal variation of zooplank-
58 ton [Ramamurthy, 1965, Piontkovski et al., 1995, Madhupratap et al., 1992, 1996a, Wishner et al.,
59 1998, Kidwai and Amjad, 2000, Barber et al., 2001, Khandagale et al., 2022] as much information
60 is revealed by later studies [Jyothibabu et al., 2010, Vijith et al., 2016, Shankar et al., 2019, Aparna
61 et al., 2022] using high resolution data. Calibrated acoustic instruments such as Acoustic Doppler

62 Current Profiler (ADCP) along with relevant data can be utilised to understand small scale vari-
63 ability [Nair et al., 1999, Edvardsen et al., 2003, Smith and Madhupratap, 2005, Smeti et al., 2015,
64 Kang et al., 2024], the complex interplay between the physico-chemical parameters and ecosystem
65 [Jiang et al., 2007, Potiris et al., 2018, Shankar et al., 2019, Aparna et al., 2022, Nie et al., 2023], the
66 zooplankton migration [Inoue et al., 2016, Ursella et al., 2018, 2021] and their seasonal to annual
67 variation [Jiang et al., 2007, Hobbs et al., 2021, Liu et al., 2022, Aparna et al., 2022].

68 1.2 ADCP backscatter and zooplankton biomass

69 At present, there are two types of acoustic samplers: non-calibrated single frequency acoustic profiler
70 such as ADCP or calibrated multi and mono frequency acoustic profilers such as zooplankton
71 acoustic profiler (ZAP) and Tracor acoustic profiling system(TAPS). The use of acoustics as a
72 proxy for zooplankton biomass estimation can be traced to Pieper [1971], Sameoto and Paulowich
73 [1977] and earlier studies which used echograms to approximate the large-scale horizontal extents
74 [Barraclough et al., 1969], and small scale vertical extent [McNaught, 1968]. The relationship
75 between backscatter and the abundance and size of zooplankton was described by Greenlaw [1979]
76 wherein it was pointed out that single frequency backscatter can be used to estimate abundance if
77 mean zooplankton size is known. This paved the way for use of single frequency acoustic profiler. A
78 drastic increase in study temporal and spatial variation of zooplankton biomass using backscatter-
79 proxy came in 1990s by introduction of high frequency echo sounders, with studies [Flagg and Smith,
80 1989, Wiebe et al., 1990, Batchelder et al., 1995, Greene et al., 1998, Rippeth and Simpson, 1998]
81 methodically showing acoustic backscatter estimated zooplankton biomass in various shelf and slope
82 locations around North Atlantic, North pacific location. The foundation for further research that
83 investigated the potential of acoustic backscatter from ADCPs and multi frequency echo sounders

84 in assessing zooplankton biomass and comprehending zooplankton dynamics in diverse maritime
85 habitats was established by these initial explorative experiments.

86 Acoustic backscatter and zooplankton biomass have been better understood as a result of tech-
87 nological and methodological developments over time. Net sampling augmented ADCP backscatter
88 have been used to study DVM and the spatial and temporal variability of zooplankton biomass in
89 different marine regions, such as the Southwestern Pacific, the Lazarev Sea in Antarctica and the
90 Corsica Channel in the north-western Mediterranean Sea [Cisewski et al., 2010, Hamilton et al.,
91 2013, Smeti et al., 2015, Guerra et al., 2019]. The zooplankton biomass variation in the Arabian
92 sea has been studied during JGOFS programme in 1990s [Herring et al., 1998, Nair et al., 1999,
93 Barber et al., 2001, Fielding et al., 2004, Smith and Madhupratap, 2005]. However, their studies
94 were limited to the cruise duration as vessel mounted ADCPs were predominantly used; hence
95 long-term data was sparsely produced. The first such study to fully exploit the immense potential
96 of ADCPs in EAS was carried out by A22 using ADCP moorings deployed on continental slopes
97 off the Indian west coasts [Amol et al., 2014, Chaudhuri et al., 2020]. A fascinating outcome of
98 A22 is the non-linear interaction between zooplankton and phytoplankton population. A22 showed
99 that the zooplankton growth in fact declines during upwelling facilitated increase in phytoplankton
100 biomass. It implies the break down of existing understanding of predator - prey relationship in
101 fundamental level of marine food chain with secondary production as a linear function of primary
102 production.

103 1.3 Objective and scope of the manuscript

104 A network of ADCPs has been installed off the continental slope and shelf on the west coast of India.
105 This ADCPs have enabled a rigorous view of intraseasonal to seasonal scale variability [Amol et al.,

¹⁰⁶ 2014, Chaudhuri et al., 2020]. Initially a network of four ADCPs (off Mumbai, Goa, Kollam and
¹⁰⁷ Kanyakumari) on continental slope, it has been extended to include three more moorings (off Okha
¹⁰⁸ from 2018, Jaigarh and Udupi from 2017). In the recent study A22 have used ADCP moorings
¹⁰⁹ off Mumbai, Goa and Kollam to explain the temporal variability of zooplankton biomass. The
¹¹⁰ study showed that the zooplankton peaks (and troughs) is not only non-uniform in latitude but
¹¹¹ also heavily influenced by the oxygen minimum zone, MLD and the seasonal upwelling/downwelling
¹¹² conditions. Stark contrast in the phytoplankton bloom and subsequence growth of zooplankton or
¹¹³ the lack thereof was observed in the EAS regimes.

¹¹⁴ We build upon the existing work by extending to include the newly incorporated ADCPs so as to
¹¹⁵ have a better understanding in the latitudinal variation of zooplankton biomass in EAS. The paper
¹¹⁶ is organized as follows; datasets and methods employed are described in detail in section 2. Section
¹¹⁷ 3 describes the observed climatology of zooplankton biomass and standing stock. A comparison is
¹¹⁸ drawn to the results of previous studies at the overlapping mooring sites. Further, the seasonal cycle
¹¹⁹ of zooplankton biomass and standing stock is discussed. The role of mixed layer depth, net primary
¹²⁰ production, sea surface temperature, wind forcing and circulation in determining the biomass is
¹²¹ discussed in results section 4, with conclusion in section 5.

¹²² 2 Data and methods

¹²³ The backscatter data from ADCP and the zooplankton samples collected from the periphery of
¹²⁴ mooring is described in this section. The methodology followed in processing ADCP data and
¹²⁵ estimation of backscatter and subsequently the zooplankton biomass is discussed. The backscatter
¹²⁶ derived from the echo intensity of the seven ADCP mooring deployed on the continental slope off
¹²⁷ the Indian west coast is the primary data we have use in this manuscript. The moorings details are

128 summarized in [Table 1](#). In situ biomass data from volumetric zooplankton samples are used to val-
129 idate and correlate with backscatter. The chlorophyll data is obtained from marine.copernicus.eu.
130 In addition, we have used the monthly climatology of temperature and salinity [[Chatterjee et al.,](#)
131 [2012](#)] and the net primary productivity from MODIS (Moderate Resolution Imaging Spectrora-
132 diometer) and VIIRS (Visible Infrared Imaging Radiometer Suite) from global NPP estimates
133 (<http://sites.science.oregonstate.edu/ocean.productivity>).

134 2.1 ADCP data and Backscatter estimation

135 The ADCPs were deployed on the continental slope off the Indian west coast ([Fig. 1](#)), off Mumbai,
136 Goa, Kollam and Kanyakumari, and later extended to three more sites to cover the entire EAS
137 basin from Okha (22.26°N) in north to Kanyakumari (6.96°N) in south. The other two ADCPs
138 are Jaigarh at central EAS (CEAS) and Udupi in the transition zone between CEAS & SEAS. The
139 extended moorings were deployed in October 2017, except for Kanyakumari which was deployed
140 earlier as well but it wasn't part of the earlier backscatter study by A22. The moorings are serviced
141 on yearly basis usually during October-November or in winter monsoon months. The ADCPs are
142 of RD Instruments make, upward-looking and operate at 153.3 kHz. While utmost care is taken to
143 position the instrument at ~ 200 m depth, yet for some deployments it's shallow or deeper owing
144 to drift caused by floater buoyancy-anchor weight balance. Data was collected at hourly interval
145 and the bin size was set to 4 m. The echoes at surface to 10 % range (~ 20 m) means the data at
146 these depths is rendered useless and is discarded from further use.

147 The procedure followed in processing of the ADCP data are described in [Amol et al. \[2014\]](#) and
148 [Mukherjee et al. \[2014\]](#). Depth correction was an addition to their methodology to accommodate
149 the vertical movement of ADCP buoys [[Chaudhuri et al., 2020](#), [Mukhopadhyay et al., 2020](#)] using

150 data from pressure sensor mounted on the instrument. We have followed the methodology laid down
151 in A22 to derive the backscatter time series from ADCP echo intensity data which is discussed later
152 paragraph. The gaps up to two days are filled using the grafting method of [Mukhopadhyay et al.](#)
153 [2020] once the zooplankton biomass time series is constructed.

154 The primary objective of ADCP usage is to obtain vertical current profile at a point location.
155 It is achieved by using the echo intensity received at the ADCP transducer. The instrument
156 sensors doesn't directly give backscatter, as echo intensity is range independent. Range correction
157 has to be performed before echo intensity (E) is converted to Backscatter (B). Received signal
158 strength indicator (RSSI), also called the conversion factor (K_c) is sensor specific and is used with
159 the corresponding reference echo intensity (E_r). It's important to state that for the same device
160 K_c remains unchanged while E_r may vary over each subsequent deployment. The backscattering
161 strength (in dB) is given by [Mullison \[2017\]](#):

$$\small{162} \quad B = [C - L_{DBM} - P_{DBW}] + 2\alpha R + 10\log_{10}[(T_{TD} + 273.16)R^2] + 10\log_{10}[10^{K_c(E-E_r)/10} - 1]$$

163 where C is an empirical constant, L_{DBM} is $10\log_{10}L$ where L is the transmit pulse length in
164 meters, P_{DBW} is $10\log_{10}P$ (P is transmitted power in watts), α is the sound absorption coefficient
165 of water (in $dB m^{-1}$), T_{TD} is the temperature (in $^{\circ}C$) at the depth of positioned instrument, R
166 is the slant range (in meters) from transducer to the scatterers and E_r is the reference level of E
167 taken in real-time (unit counts). E_r in our case is taken from first (last) measured profile when the
168 instrument is in air before (after) deployment (retrieval). The backscattering strength is referenced
169 to $(4\pi m^{-1})$ [[Deines, 1999](#), [Mullison, 2017](#)]. A22 has discussed the relevance of each of the term to
170 the total backscattering strength. Our analysis also suggests that the α does not affect the final
171 results.

172 **2.2 Zooplankton data and estimation of biomass**

173 The zooplankton samples were collected in the vicinity (~ 10 km) of ADCP mooring site twice; once
174 prior retrieval and again post deployment of moorings so that there is overlap in the ADCP time
175 instance and in situ zooplankton samples. The sampling is done at the mooring location during
176 servicing cruises on board RV Sindhu Sankalp and RV Sindhu Sadhana (Table 2). Multi-plankton
177 net (MPN) (100 μm mesh size, 0.5 m^2 mouth area) was used to get samples in the pre-determined
178 depth ranges; water volume filtered was calculated by the product of sampling depth range and the
179 mouth area of net. The depth range and timing of sample collection was different throughout the
180 MPN hauls (refer [Table 2](#)). From 2020 onward, the depth-range was standardized to the bins of 0
181 – 25, 25 – 50, 50 – 75, 75 – 100, 100 – 150 (units are in meters). The collected zooplankton samples
182 were then preserved in 5 % formaldehyde solution until it's transferred to laboratory. To measure
183 zooplankton wet weight accurately, the gelatinous forms/salps were separated. A22 had reported
184 the calanoid copepods, cyclopoid copepods, Poecilostomatoida, Harpacticoida, appendicularians,
185 euphausiids, ostracods, and chaetognaths as the major groups of zooplanktons contributing to the
186 biomass of net samples from the mooring sites. The backscatter obtained earlier is averaged in
187 vertical corresponding to the specific MPN hauls for each site. The backscatter is linear regressed
188 with respective biomass to establish their relationship, which has been demonstrated in numerous
189 previous studies [Flagg and Smith, 1989, Heywood et al., 1991, Jiang et al., 2007, Aparna et al.,
190 [2022](#)].

191 We calculated the regression equation to be $y = 0.0203 x + 4.01$ and, which is well within the
192 error range of the regression equation of A22, $y = (0.02 \pm 0.004) x + (4.14 \pm 0.36)$ with a correlation
193 of 0.53 ([Fig. 2](#)). The correlation value in our case is 0.54; the minor difference is due to higher
194 number of data points (159) in the present study compared to A22 (67).

195 **2.3 Biomass time series and estimation of standing stock**

196 The zooplankton biomass time series ([Fig. 3](#)) is created from the above derived linear relationship:

197 $Bm = m * Sv + k$

198 where Bm is biomass taken in \log_{10} scale, m is slope, Sv denotes backscattering strength and
199 k is the intercept. The time series shows the pattern of diel vertical migration (DVM) at all the
200 mooring sites during dawn (\sim 0600-0700 hours) and dusk (\sim 1800-1900 hours). It is evident in earlier
201 studies using backscatter [[Ashjian et al., 2002](#), [Smith and Madhupratap, 2005](#), [Inoue et al., 2016](#),
202 [Ursella et al., 2018](#)] and in situ zooplankton data [[Padmavati et al., 1998](#)]. The implication of DVM
203 is a higher biomass at surface during the night as zooplankton feeds and a lower biomass at daytime
204 as they descend to subsurface depths. The overall biomass over the time period of a day may vary
205 but the DVM doesn't affect the seasonal variation as shown by [Jiang et al. \[2007\]](#) and A22. Since
206 our goal is to study the seasonal variation, delineating the daily biomass is sufficient. The biomass
207 time series and it's seasonal cycle is discussed in ??.

208 The standing stock is determined by taking the depth integral of biomass over the water column.

209 To maintain the consistency of standing stock estimation, only those deployments that doesn't lack
210 data at any depth in the entire range of 24 – 120 m are considered for analysis as in A22. The lack
211 of data in the above mentioned depth range is due to deviation in positioning of ADCP sensor in the
212 water column. A swift alteration in bathymetry along the continental slope implies that the mooring
213 might anchor at a different depth than planned, hence a change in the predicted position of ADCP.
214 This leads to gap in data at few mooring sites for some year. For example, for the northern-most
215 mooring at Okha, data is not available for the entire upper 120 m depth for the second deployment.
216 Also at Jaigarh, where the surface to \sim 60m data (in 3rd deployment) and Kollam, where 80 m
217 and below (in 4th deployment) is unavailable and hence discarded from standing stock estimation.

218 There are few deployments where no data or bad data was recorded e.g, at Udupi (4th deployment)
219 and Kanyakumari (6th deployment). The seasonal cycle of standing stock for 24 – 120 m available
220 data is explored in ??.

221 Through the findings of biomass variability in different time scale, we hypothesize that current
222 may influence the zooplankton biomass by driving nutrients and phytoplankton rich water. Wavelet
223 coherence between current and biomass is taken for each depth, and from this data, the coherence
224 and phase at annual period is taken to check for dependency of biomass on current. In section 5
225 we shed a light on possible dependency of biomass on zonal & meridional current.

226 2.4 Mixed-layer depth, temperature and oxygen

227 As we are using a 153.3 kHz ADCP moored at ~ 150 m, the top ~ 10% of data is unusable because
228 of surface echoes. MLD in EAS is of the order ~ 20 to 40 m during summer monsoon [[Shetye et al., 1990](#), [Sreenivas et al., 2008](#)] especially in the SEAS, but during winter the MLD in northern
229 NEAS remains deep [[Shankar et al., 2016](#)]. Although it is possible to use the near-surface ADCP
230 data after due noise correction; it is beyond the scope of present study. The temperature data is
231 used from [Chatterjee et al. \[2012\]](#), a monthly climatology having 1 ° spatial resolution. Monthly
232 climatology of oxygen data is obtained from World Ocean Atlas 2013 [[García et al., 2014](#)] which
233 contains objectively analyzed 1 ° climatological fields of in situ measurements.
234

235 2.5 Chlorophyll and net primary productivity data

236 Previous study based on ADCP data of EAS A22 have used SeaWiFS based chlorophyll data for
237 comparison with climatology of zooplankton standing stock (ZSS). The SeaWiFS was at its end
238 of service in 2010, hence we use new chlorophyll product. The present study has been conducted

²³⁹ using Global Ocean Colour, biogeochemical, L3 data obtained from the [E.U. Copernicus Marine](#)
²⁴⁰ [Service Information](#). The daily data is available at a spatial resolution of 4 km.

²⁴¹ While chlorophyll is used to compare with the variation in climatology of zooplankton standing;
²⁴² the growth efficiencies of zooplankton are directly linked to primary production levels, emphasizing
²⁴³ the interconnectedness between primary producers and consumers in marine food webs [[Friedland](#)
²⁴⁴ [et al., 2012](#)]. In their study, A22 has emphasized on the collapse of the predator-prey relationship
²⁴⁵ between zooplankton-phytoplankton using climatological data. We showcase their interdependency
²⁴⁶ or the lack thereof using net primary productivity models. Moderate Resolution Imaging Spectro-
²⁴⁷ radiometer (MODIS) based net primary productivity (NPP) data at a resolution of $0.16^\circ \times 0.16^\circ$
²⁴⁸ was obtained from Oregon State University. They have employed three different schemes to obtain
²⁴⁹ NPP from Chlorophyll concentration. Those are discussed below in brief. The first is Vertically
²⁵⁰ Generalized Production Model (VGPM). The NPP (a rate term) is to be derived from chlorophyll
²⁵¹ (a standing stock) using chlorophyll-specific assimilation efficiency for carbon fixation. The single
²⁵² biggest unknown in all models based on chlorophyll is how this rate term is described. VGPM
²⁵³ considers the primary productivity to be dependent on day length and maximum daily NPP within
²⁵⁴ a water column. The second is Carbon-based Productivity Model (CbPM) which NPP to phy-
²⁵⁵ toplankton carbon biomass and growth rate. The third is Carbon, Absorption, and Fluorescence
²⁵⁶ Euphotic-resolving (CAFE) mode; first described in [Silsbe et al. \[2016\]](#) takes various other factors
²⁵⁷ into NPP calculations. We explore these NPP models and try to explain the variation in ZSS.

²⁵⁸ **3 Climatology of zooplankton biomass and standing stock**

²⁵⁹ The previous study of zooplankton in EAS based on ADCP backscatter was consisting of three
²⁶⁰ sites: Mumbai in NEAS, Goa in CEAS and Kollam in SEAS. The extended mooring sites are at

²⁶¹ Okha at NEAS, Jaigarh at CEAS, Udupi in the transition zone of CEAS & SEAS and Kanyakumari
²⁶² at SEAS is the southern most location in our study area.

²⁶³ ADCP data from three mooring sites were analysed from 2012 to 2020 in A22. They have
²⁶⁴ fine-tuned the methodology to obtain backscatter and estimated zooplankton biomass from it using
²⁶⁵ in situ volumetric zooplankton biomass data. A comparison is made in later paragraphs, since the
²⁶⁶ methodology remains same in the current study and new time series data is available. The monthly
²⁶⁷ climatology of biomass and ZSS is computed for all locations having valid data in 24 – 140 m depth
²⁶⁸ range ([Fig. 4](#)).

²⁶⁹ The high biomass regime in the upper ocean and low biomass regime in deeper depths is differ-
²⁷⁰ entiated using a biomass contour: 215 mg m^{-3} off Mumbai, Goa, Kollam, Jaigarh and Udupi, 175 mg m^{-3} off Okha and Kanyakumari. For simplicity, this biomass contour is abbreviated to be z215
²⁷¹ & z175 and its depth is denoted as D215 & D175, respectively. The choice of biomass contour isn't
²⁷² abrupt; first, it is carefully chosen to accommodate the seasonal variation, as a shift to biomass
²⁷³ contour lower than the z215 would be unviable as our data is only till 140 m depth, for example in
²⁷⁴ the case of Kollam, the D215 exceeds 140 during few months of 2022 ([Fig. 3](#)). A higher biomass
²⁷⁵ contour would lead to inferior view of the seasonal cycle as in the case of Kanyakumari and Okha
²⁷⁶ where 215 mg m^{-3} biomass contour is often low enough to reach $\sim 20 - 30 \text{ m}$ depths, hence z175 is
²⁷⁷ chosen here. Second, it allows us to link the seasonal variation of biomass to the physico-chemical
²⁷⁸ properties.

²⁸⁰ The climatology of zooplankton biomass and ZSS ([Fig. 4](#)) is discussed at locations northward
²⁸¹ starting from southernmost mooring site off Kanyakumari.

282 **3.1 Southern EAS**

283 During mid-march off Kanyakumari, the depth of 23°C isotherm (henceforth D23) shallows along-
284 with oxycline (marked by 2.1 ml L^{-1}) and a rise in biomass is observed ([Fig. 4 g1](#)). The z175
285 is shallower from May onward to October and the zooplankton biomass is comparatively higher
286 than rest of the year. The D175 deepens starting from October and the relatively high biomass in
287 water column is maintained till late December. However, this increase in D175 isn't reflected as an
288 increase in ZSS because of low biomass in the entire water column. A gradual increase is seen in
289 the chlorophyll biomass starting from April and the peak is attained in June ([Fig. 4 g2](#)). The ZSS
290 is increased in June, however the growth is minimal. There is almost no seasonal variation in ZSS
291 off Kanyakumari (ZSS std, 0.67 gm m^{-2}) as compared to the ZSS variation at the nearest northern
292 mooring site off Kollam (ZSS std, 1.25 gm m^{-2}), where a strong seasonal cycle is observed and the
293 D215 is deeper for any given month.

294 Off Kollam, a higher biomass is present in the larger portion of water column and the D215 is at
295 $\sim 110\text{ m}$ during Mar-May ([Fig. 4 f1](#)). Similar to z175 off Kanyakumari, the decrease in biomass with
296 depth is subtle below z215. Starting from March, the D215 begins to shallow with progress in time
297 till August. During this period, a sharp decrease is seen in the D23 ($\sim 80\text{ m}$ in June to September)
298 while the oxycline (1.7 ml L^{-1}) overshoots the thermocline ([Fig. 4 f1](#)). A steep rise in chlorophyll
299 biomass is seen off Kollam and its peak is attained in August ([Fig. 4 f2](#)). The ZSS declines in the
300 same period and reaches a minimum when the chlorophyll biomass is at its peak. The chlorophyll
301 biomass decreases rapidly in the following months, while the ZSS increases and a maximum is seen
302 during October. This feature was earlier reported by A22 showing disproportionate interaction
303 between zooplankton and phytoplankton. A similar feature is seen further north, off Udupi which
304 sits at the transition zone of SEAS & CEAS, albeit with a relatively weaker zooplankton biomass.

305 The peak of chlorophyll and minimum of ZSS occurs in September ([Fig. 4 e2](#)) which is one month
306 later than off Kollam. The 2.1 ml L^{-1} oxygen contour overshoots thermocline, however it reaches to
307 a much shallow depth of $\sim 20 \text{ m}$ during July to October unlike any other location in our EAS study
308 area. The D215 vaguely follows D23; with the gradual shallowing from March onward reaching
309 $\sim 60 \text{ m}$ in September and a steep decline afterwards till November ([Fig. 4 e1](#)). The decrease of
310 biomass with depth is moderate in comparison to Kollam.

311 **3.2 Central EAS**

312 Off Goa, the D215 seasonal trend is similar to Udupi and is entirely restricted by D23 & 1.7 ml L^{-1}
313 oxygen contour that closely follows it. During March-May, the D215 is at $\sim 80 - 100 \text{ m}$ which
314 shallows with onset of summer monsoon ([Fig. 4 d1](#)); the chlorophyll biomass increases during this
315 period and the maximum occurs in August after which the chlorophyll biomass and ZSS ([Fig. 5](#))
316 both decrease in September. Although we witness an increase in chlorophyll biomass in October,
317 the D215 is restricted to the $\sim 50 \text{ m}$ in this period and the ZSS is at its minimum similar to what
318 is observed off Udupi (Kollam) during September (August). The ZSS rapidly increases and reaches
319 its maximum in January, sustained till March and then gradually declines. Unlike the previous
320 locations, the biomass off Goa decreases rapidly below the z215 as reported earlier in A22, reaching
321 as low as 60 mg m^{-3} at 130 m during June to September ([Fig. 4 d1](#)).

322 The ZSS off Jaigarh is identical but stronger to that of off Goa, owing to a higher biomass
323 above z215 and the comparatively deeper D215 ([Fig. 4 c1](#)). The D215 follows D23 & oxycline
324 for most of the year and it only exceeds during October-December. From the ZSS maximum in
325 February ([Fig. 4 c2](#)), it steadily decreases and attains a minimum in September (coincides with
326 lower D200), a rapid rise is seen in the following months. What's intriguing is a presence of strong

327 seasonal cycle in ZSS off Jaigarh (ZSS std 3.24 gm m^{-2} , highest among all locations) although the
328 seasonal variation in chlorophyll biomass ([Fig. 4 c2](#)) is visibly non-existent (Chl std, 0.05 mg m^{-3} ,
329 lowest among all locations). This is an exact opposite scenario of Kanyakumari site, where an
330 insignificant seasonal variation in ZSS (ZSS std, 0.67 gm m^{-2}) is seen even though the chlorophyll
331 biomass varies strongly (chl std, 0.51 mg m^{-3}).

332 Starting from Kollam ([Fig. 4 f1](#)) and moving northward to Jaigarh ([Fig. 4 c1](#)), we see that the
333 core of high zooplankton biomass gradually shifts from summer monsoon (off Kollam) to winter
334 monsoon (off Jaigarh), with the transition of upper ocean zooplankton biomass happening along
335 Udupi and Goa. On the contrary, the chlorophyll biomass tends to have low seasonal range as we
336 move northward from SEAS, with Jaigarh having the least seasonal variation.

337 3.3 Northern EAS

338 Further north of Jaigarh, off Mumbai the D215 follows a similar pattern i.e, a deeper D215 in
339 December to early April, resulting in a higher ZSS in the same period ([Fig. 4 b2](#)). The D23 off
340 Mumbai follows D215 and the oxycline follows an erratic pattern, reaching depths > 140 during
341 January to March ([Fig. 4 b1](#)); when a higher biomass is observed above z215. The chlorophyll
342 biomass shows seasonal variation albeit lower than the SEAS counterpart. Its peak occurs in
343 August, then decreases rapidly and increases from October onward maintaining the biomass at 0.5
344 mg m^{-3} till March. In zooplankton biomass climatology, during September-October a thin layer
345 of low biomass regime is seen at depths $\sim 30 - 40$ m, combined with shallow D215 resulting in a
346 ZSS minimum. The ZSS increases rapidly from its minima in October in the following month as
347 the D215 deepens and the maximum occurs in February. The chlorophyll biomass decreases from
348 March and a gradual decrease in ZSS is seen till July, after which the ZSS basically flattens even

349 though the chlorophyll increases.

350 At the northernmost site of EAS i.e, off Okha, a noticeable feature is a much higher oxygen in
351 upper ocean except during summer monsoon. The biomass above z200 is much weaker ([Fig. 4 a1](#))
352 compared to Mumbai as seen in the zooplankton biomass climatology which leads to a relatively
353 lower ZSS ([Fig. 4 a2](#)). The D200 shallows from February (coinciding with ZSS maximum) to it's
354 minimum in August, remains visibly flat till September and then increases steadily till December
355 and rapidly afterwards. There's two chlorophyll peak off Okha; one in February [[Keerthi et al., 2017](#),
356 [2017](#)] and the other during August in summer monsoon [[Lévy et al., 2007](#)]. The ZSS remains flat
357 in summer monsoon period i.e, June to September, although the chlorophyll biomass increases in
358 this time. Afterwards, ZSS gradually increases and attains its maximum in February same as the
359 chlorophyll biomass. The ZSS sustains this maximum till March, declines rapidly in April and then
360 gradually till July.

361 3.4 Comparison to biomass and ZSS climatology of A22

362 A comparison with the zooplankton biomass and standing stock climatology of previous work A22
363 is made in this section for the locations of Mumbai, Goa and Kollam. In the previous study data
364 from 2012 to 2020 is used, while the present study includes data from 2017 to 2023.

365 It is observed that D215 is shallower at all locations and as a result a lower ZSS is seen in the
366 climatology of the present study ([Fig. 5](#)). The difference in D215 is prominent off Goa; while in the
367 previous climatology ([Fig. 5 b1](#)) the D215 is deeper and lies along D23, in the present climatological
368 data ([Fig. 5 b2](#)) the D215 is shallower and lies $\sim 20 - 40$ m above the D23 during January to April.

369 A relatively lower biomass is present above z215 year round which reflects in overall lower ZSS.
370 This goes same for the biomass off Mumbai ([Fig. 5 a1 & a2](#)) i.e, a comparatively shallow D215

371 and lower ZSS in comparison with A22. Instead of a ZSS maxima in February, in the present data,
372 the maxima is sustained in march, which could be due to the lower value of ZSS in February. The
373 second maxima occurs in August ([Fig. 5 d1](#)) which is less pronounced in recent data ([Fig. 5 d2](#)).
374 Similar to Goa, there is dramatic decrease in the minima that occurs in October and ZSS increases
375 rapidly post October till February. Off Kollam, a higher biomass is observed from May to June in
376 A22, while in the present study, along with May to June, a higher biomass is seen from September
377 to November([Fig. 4 c2](#)) which is reflected as a minima of ZSS occurring in August ([Fig. 4 d2](#)). The
378 higher ZSS on either side to this minima is less pronounced in A22. This difference in ZSS is clearly
379 seen in the correlation, which is 0.60 off Kollam, while it is 0.94 and 0.98 off Mumbai and Goa,
380 respectively. Note that the correlation only shows how similar the ZSS trend is and doesn't tell
381 us about the deviation in magnitude w.r.t. time. Chlorophyll biomass shows stronger peak for all
382 locations in August in present study, when the zooplankton-phytoplankton relationship discrepancy
383 is observed off Kollam similar to results reported in A22.

384 4 The biomass time series and seasonal cycle

385 In this section we will describe the zooplankton biomass time series followed by a discussion on the
386 seasonal cycle and variability.

387 4.1 Time series of zooplankton biomass

388 Biomass contour to demarcate upper (high biomass) to lower (low biomass) regimes is devised for
389 each zooplankton time series to show their seasonality. A preliminary analysis of the biomass time
390 series in daily and monthly averaged scale shows that the biomass decreases with increasing depth
391 ([Fig. 3](#)) at all the seven locations. The rate of biomass decrease with depth, roughly defined as the

difference between the mean biomass at 40 m and 104 m depth, is highest off Jaigarh and Mumbai as it has higher biomass in upper ocean ([Fig. 6 c,b](#)). This is followed by CEAS locations Goa and Udupi ([Fig. 6 d,e](#)). While the biomass decrease with depth is lower off Kollam from 2017 to 2020, it becomes considerably high from thereon ([Fig. 6 f](#)). The rate of decrease is lowest off Kanyakumari. The mean of biomass, standard deviation of zooplankton biomass, ZSS and chlorophyll is shown in [Table 3](#). Following poleward along the slope, the mean biomass at 40 m off Kanyakumari is the least $\sim 207 \text{ mg m}^{-3}$ which increases drastically to 272 mg m^{-3} off Kollam. It decreases till Goa and then increases to a maximum of 278 mg m^{-3} off Jaigarh. Off Mumbai the mean biomass is 272 mg m^{-3} , and further north off Okha, it declines to 230 mg m^{-3} . A similar trend is observed in mean biomass at 104 m depth of all locations and their corresponding standard deviation. A pattern that develops from this is observed, with lower mean biomass off Okha (northernmost of EAS) and off Goa (CEAS) bifurcated by higher mean biomass off Mumbai & Jaigarh; while the lower mean biomass off Udupi (CEAS) and off Kanyakumari (Southernmost of EAS) is divided by higher mean biomass off Kollam. Similarly, from standard deviation of biomass it is inferred that the sites with higher biomass tends to have higher variation over time as in the case of Mumbai, Jaigarh and Kollam.

A comparatively weaker decline in zooplankton biomass with respect to depth off Okha ([Fig. 3 a1,a2](#)) at NEAS is agreeing with earlier reported data [[Wishner et al., 1998](#), [Madhupratap et al., 2001](#), [Smith and Madhupratap, 2005](#), [Jyothibabu et al., 2010](#)] where oxygen deficit is thought to be the cause, particularly during summer monsoon seen in [García et al. \[2014\]](#) climatology (figure not shown). The sites at SEAS, especially off Kanyakumari and 2017 to 2020 off Kollam also have weaker decrease [[Madhupratap et al., 2001](#), [Jyothibabu et al., 2010](#), [Aparna et al., 2022](#)]. However, post 2020 the decline in biomass with depth off Kollam is similar to that off Mumbai in stark

415 contrast to its previous years owing to a strong bloom in these years. This growth is reflected as
416 an increase in biomass in the entire water column ([Fig. 3 f1,f2](#)) and deepening of D215. Analyzing
417 the demarcating biomass contours (z175, z215 of respective locations) we see a strong seasonality
418 at NEAS, CEAS and SEAS (excluding Kanyakumari), although a shallow and seasonally invariant
419 D215 is seen for Goa and Kollam during January 2019 to December 2020. While the z175 and
420 z215 is deeper in winter monsoon throughout EAS, at the NEAS regime, the upper ocean shows
421 considerably high biomass during this period as in the case of Okha, Mumbai and Jaigarh. On the
422 contrary, at SEAS regime the upper ocean shows higher biomass during summer monsoon as seen
423 off Udupi, Kollam and Kanyakumari even though the D215 & 175 is shallower in this period.

424 **4.2 Seasonal cycle of biomass and standing stock**

425 The zooplankton standing stock time series is obtained by integrating the biomass over 24 – 120 m
426 of water column, ([Fig. 9](#)). The presence of significant variation in the 30-day running mean with
427 recurring burst is seen in the daily data. In NEAS regime, the ZSS maximum occurs during January
428 to late march and early April as seen off Okha, Mumbai, Jaigarh and Goa. However, the decline of
429 ZSS post the maxima is comparatively gradual off Goa which was also visible in the climatology of
430 ZSS ([Fig. 4 d2](#)). The growth in ZSS at NEAS sites during summer monsoon is much lower compared
431 to the SEAS. For example, off Kollam, we observe the presence of double peak, one during May to
432 July and the another during September to November. Similar feature is seen off Udupi, the nearest
433 northern site of Kollam, but with a much higher ZSS during September to November as compared
434 wit May to July ZSS. Off Kanyakumari, although there seems to be intra-annual variations, a clear
435 annual cycle is not observed.

436 The zooplankton standing stock time series is obtained by integrating the biomass over 24 –

437 120 m of water column, ([Fig. 9](#)). The presence of significant variation in the 30-day running mean
438 with recurring burst is seen in the daily data. In NEAS regime, the ZSS maximum occurs during
439 January to late march and early April as seen off Okha, Mumbai, Jaigarh and Goa. However,
440 the decline of ZSS post the maxima is comparatively gradual off Goa which was also visible in
441 the climatology of ZSS ([Fig. 4 d2](#)). The growth in ZSS at NEAS sites during summer monsoon is
442 much lower compared to the SEAS. For example, off Kollam, we observe the presence of double
443 peak, one during May to July and the another during September to November. Similar feature is
444 seen off Udupi, the nearest northern site of Kollam, but with a much higher ZSS during September
445 to November as compared with May to July ZSS. Off Kanyakumari, although there seems to be
446 intra-annual variations, a clear annual cycle is not observed.

447 4.2.1 The annual cycle

448 The time series has loss of data due to instrument fault or improper position of ADCP in the
449 water column. For example, off Okha during it occurred in the second deployment (Dec-2019 to
450 Dec-2020), the instrument was way below from its intended depth of 150 m leading to no data in
451 top 140 m water column. It is not possible to construct a continuous record and hence it makes
452 it difficult to interpret the annual cycle where ever the data record is short. So, for 40 m biomass
453 time series we restrict our description to all locations except Okha and Jaigarh while performing
454 wavelet analysis.

455 Off Mumbai, a strong annual cycle (~ 365 days) dominates the seasonal cycle throughout the
456 time series ([Fig. 7 b](#)). Annual cycle is comparatively weak off Goa (CEAS) contrary to results of
457 A22 which could be due to shorter time record and low biomass in the recent years. The annual
458 cycle off Udupi & Kollam (SEAS) is strong, however it varies in time and off Kollam the wavelet

459 power is stronger post 2020 ([Fig. 7 f](#)). Further south, off Kanyakumari, the annual cycle weakens
460 having power similar to that of Goa. At 104 m, the annual cycle strengthens off Mumbai and Goa
461 ([Fig. 8 b, d](#)) compared to the annual cycle at 40 m; implying that the biomass seasonal variation
462 at 104 m is robust even though the mean biomass is considerably lower. Annual cycle weakens off
463 Kollam ([Fig. 8 f](#)), although only vague interpretation can be made as it lies beyond the cone of
464 influence.

465 The absence of ZSS annual cycle off Kanyakumari is confirmed with wavelet analysis ([Fig. 9](#)
466 g1). Off Kollam, the presence of an weak annual cycle in ZSS is seen contrary to a strong annual
467 cycle of Udupi, however a longer data record is needed as the annual period lies beyond the cone of
468 influence. Off Goa ([Fig. 9 d1](#)), the annual cycle was weak for 2018 to early 2020, which strengthened
469 afterwards. The ZSS annual cycle is strongest off Mumbai ([Fig. 9 b1](#)) throughout the data record
470 and the wavelet power is highest among all locations. Analysis reveals the presence of strong annual
471 cycle off Jaigarh and Okha.

472 **4.2.2 The semi-annual cycle**

473 Along with the annual cycle, we observe presence of semi-annual (~ 180 days) cycle at most locations
474 and together they constitute the seasonal cycle. At 40m depth Off Okha the semi-annual period is
475 weak. Off Mumbai however, the semi-annual cycle is present throughout the record and becomes
476 stronger in 2022-2023 ([Fig. 7 b](#)) but not as much as the annual cycle. At Goa we see that the
477 semi-annual period dominates seasonal cycle in the same duration ([Fig. 7 d](#)). The dominance
478 of semi-annual cycle is also seen off Kollam. Although the dominance of semi-annual period in
479 seasonal cycle is seen only for some years, a similar feature was discussed for WICC where the
480 intra-annual component dominates the seasonal cycle as we go equatorward with a change in the

481 strength of intra-annual component in time [Chaudhuri et al., 2020]. However, off Kanyakumari
482 the semi-annual cycle is absent ([Fig. 7 g](#)).

483 Unlike the annual band which becomes stronger at 104 m, the semi-annual band weakens off
484 Mumbai & Goa at the same depth ([Fig. 8 b,d](#)). While the semi-annual band at 104 m becomes
485 relatively stronger compared to the semi-annual band at 40 m off Okha ([Fig. 8 a](#)), it is almost
486 non-existent off Kanyakumari ([Fig. 8 g](#)). The wavelet power of semi-annual cycle is same at 40 m &
487 104 m off Mumbai, Goa and Kollam for most of the data record, but weakens at 104 m compared to
488 40 m during 2022. Investigating the longer time series off Mumbai, Goa and Kollam, it is observed
489 that the semi-annual cycle is comparable to the annual cycle at some instances such as in 2022 and
490 the it strength increases as we move equatorward.

491 The ZSS annual cycle off Kanyakumari is absent, however, wavelet analysis shows presence
492 of a semi-annual cycle from early 2019 to late 2021([Fig. 9 g1](#)). This semi-annual feature is seen
493 off Kollam ([Fig. 9 f1](#)) with moderate power and with a much higher power off Udupi ([Fig. 9 21](#))
494 during 2018 to 2020. Much like the annual cycle off Goa, it's semi-annual period is weak to nearly
495 non existent before 2020 and gets strengthened afterwards. Off Mumbai, the semiannual period
496 is present from late 2018 to late 2020 and from 2022 onward. Fourier analysis shows that the
497 semi-annual cycle off Udupi is comparable to its counterpart off Mumbai during the same period.

498 The higher beta (β) coefficients off Jaigarh and Kollam implies a significant contribution of
499 low frequency variability (higher period) is more compared to the high frequency variability and is
500 discussed in detail in later section. In fact, a biennial peak is seen off Kollam in the Fourier analysis
501 even with a 3 year record agreeing with earlier findings of A22, i.e, Kollam having a weak (strong)
502 annual (biennial) cycle.

503 **5 Annual, intra-annual and intraseasonal variability**

504 The biomass at a given instance is decomposed to several exclusive period bands spanning days to
505 months. DVM is the simplest variation (low period or high frequency) among many that determines
506 zooplankton biomass at a given depth, with higher (lower) biomass during night (day) at the surface
507 regime for a number of species. Our focus, however is on the variability occurring in the higher
508 period (lower frequency) bands namely, annual, intra-annual and intraseasonal variability.

509 The strength and contribution of distinct components of variability differs in time and between
510 different regimes of EAS. For example, during 2019 off Kollam at 40 m depth, the variability in
511 shorter time scale (days to weeks) is dominated by high frequency components (< 30 days) ([Fig. 10](#)).
512 The contribution of high frequency components to the total biomass was evident in the beta value
513 in Fourier analysis, larger beta value implying a bigger contribution of the high frequencies than
514 the lower ones. An increase in biomass during summer monsoon of 2019 is facilitated by the low
515 frequency variability. However, during August a sharp decline in biomass is observed and the
516 decomposition of variability suggests that it is due to a decrease in intra-annual and intra-seasonal
517 variability even though the annual variability was weakly positive.

518 **5.1 Annual variability**

519 To capture the annual variability, the biomass is filtered with lanczos filter within period of 300 to
520 400 days. The annual variability shows that the contribution of this band to the time series of total
521 biomass is very weak. The annual variability off Kanyakumari (standard deviation 3.64 mg m^{-3})
522 and Okha (3.73 mg m^{-3}) is low, while it is stronger at rest of the basin, with strongest variability
523 off Jaigarh (9.05 mg m^{-3}). Similar to the ocean currents [[Amol et al., 2014](#), [Chaudhuri et al., 2020](#)],
524 the annual filtered biomass decreases strongly with depth off Kollam than off Mumbai and the three

CEAS sites (Fig. 11). Upward phase propagation in zonal and meridional current is observed at almost all mooring sites and also seen in the annual filtered biomass time series, i.e, off Goa and it's southern mooring sites. Owing to the above, advection as a driver to upwelling and further as one of the cause for zooplankton growth is hypothesized and their relationship is explored. Wavelet coherence shows that the current and biomass have strong coherence off Kanyakumari (2019,2021), Kollam (2019, 2022) during May to late summer monsoon of 2019 with meridional current leading biomass, when the currents are reversing with monsoon (Fig. 12). As we go poleward along the slope, coherence exists but at different depth i.e, off Goa for 2019, the maximum coherence of meridional current with biomass is at 50 to 80 m and again below 110 m. The feature observed in annual filtered biomass off Goa is similar to the alongshore component [Nethery and Shankar, 2007], with the core of biomass and alongshore current lying at about 50 m. Further north, off Mumbai a shift in time of maximum coherence is observed occurring in winter monsoon at 80 m and below with zonal current leading biomass. During pre-summer monsoon upwelling sets as early as February in SEAS but only in May farther north along the coast [Banse, 1968, ?] which results in shift in biomass coherence as we go poleward. Off Okha however, present of coherence is seen throughout 2021 from 20 to 150 m with meridional current leading biomass which could be due to a deeper MLD in northern NEAS [Marra and Barber, 2005, Shankar et al., 2016]. This has implications on the nature of zooplankton and fisheries found in regimes of EAS as we'll discuss.

5.2 Intra-annual variability

The variability at intra-annual (100 – 250 days) band tends to be stronger compared to the annual variability and is strengthened during late summer monsoon to transitional monsoon months (Fig. 13) as seen during 2018, 2019 and 2022. The higher variability often coincides with shallow

547 D215/D175, for example off Goa during 2020 and 2022, and weak variability coincides with constant
548 depth of D215. Intra-annual variability of biomass increases equatorward with higher variation seen
549 off Goa, Udupi and Kollam; although off Kanyakumari the variability is reduced. However, Fourier
550 analysis of the daily biomass time series suggests presence of signals within the intra-annual band
551 off Kanyakumari, e.g, power peaks at \sim 140 and \sim 220 days implying that the variability is strictly
552 restricted to narrow bands within intra-annual band. There is a significant variation in the strength
553 of intra-annual variability ([Fig. 13](#)) and its component ([Fig. 7](#)) with time. For example, off Goa at
554 40 m during September to November of 2020 and 2022, the intra-annual component is weak and
555 strong, respectively ([Fig. 13](#)). This difference is due to the spread of energy among all intra-annual
556 periods for 2022 ([Fig. 7](#)), while during 2020 the wavelet energy is only present in the semi-annual
557 periods, resulting in a overall weaker intra-annual component. For the same reason, the intra-annual
558 variability is non-existent in 2019.

559 **5.3 Intraseasonal variability**

560 The intraseasonal band, defined as the variability occurring between periods of few days to 90
561 days is split into two categories; a high-frequency (period $<$ 30 days) and a low-frequency (30 $<$
562 period $<$ 90 days) component. The presence of low-frequency intraseasonal signals is observed in
563 the wavelet analysis of biomass at 40 m ([Fig. 7](#)) and 104 m ([Fig. 8](#)) as bursts during few months
564 distinctive to each mooring location. The wavelet power at 40 m in low-frequency intraseasonal
565 band peaks during September to December off Mumbai, Jaigarh and Kanyakumari while no such
566 general observation is found in other locations. However, the wavelet power at 104 m in comparison
567 to 40 m suggests a decrease in its strength at respective locations. Lanczos filtered biomass in 30 to
568 90 day period shows that the intraseasonal variability is strong during August to November off all

location (Fig. 14). This is in contrast to the WICC intraseasonal band which is strong during winter monsoon [Amol et al., 2014, Chaudhuri et al., 2020]. The low frequency intraseasonal variability is higher in the upper ocean, however it can extend to deeper depths (~ 140) for some years e.g, off Kollam during 2022 (Fig. 14 f). The magnitude of low-frequency intraseasonal component is high as we move equatorward till Kollam and declines off Kanyakumari (Fig. 14 g). As noted earlier in variability of the intra-annual component, the intra-seasonal component is transient and its magnitude is higher than the low frequency variabilities. A strong dependency of zooplankton biomass on the intra-seasonal variation has implication on the sampling of zooplankton.

6 Discussion

Numerous factors have an impact on the zooplankton population dynamics and growth in the EAS. Throughout the summer monsoon, the Somali current, which flows clockwise in Arabian sea, is essential in moving oxygen-depleted waters creating a perennial oxygen minimum zone (OMZ) [Sarma et al., 2020, Sudheesh et al., 2022]. The net transport of water in upper 500 m of northern Arabian sea is about 5 Sv and a majority of the replaced waters comes from upwelling in the eastern Arabian sea [Shi et al., 1999] during summer monsoon with the high-nutrient water covering ~ 500 -700 km from coast [Morrison et al., 1998]. Upwelling supplies nutrients to the surface [Kumar et al., 2000], but it also plays a role in the creation of hypoxic conditions, which can restrict the kinds of zooplankton species that can survive in these waters [Jayakumar et al., 2004]. The upwelling starts in early by February itself off SEAS, but it occurs much later during May farther north along the coast [Banse, 1968, Kumar et al., 2000, Vijith et al., 2016, Sarma et al., 2020] albeit weaker than the southern counterpart. The deepening of MLD in winter due to convective mixing during [Marra and Barber, 2005, Shankar et al., 2016, Shi and Wang, 2022] leads to dilution of zooplankton grazers

591 in water column [Marra and Barber, 2005] and hence longer food chain [Banse, 1995, Barber et al.,
592 2001], explaining the carnivore dominated fisheries in NEAS [Shankar et al., 2019] and planktivore
593 dominated SEAS [Longhurst and Wooster, 1990, Shankar et al., 2019].

594 The southwest monsoon was found to be the most productive period [Kumar et al., 2000]
595 however the observed primary productivity values were lower than predicted primary productivity
596 owing to efficient grazing by mesozooplankton that kept diatom biomass in check instead of high
597 levels of primary productivity as seen in coastal upwelling regions [Barber et al., 2001]. Similar
598 to the zooplankton variability, the inter-annual variability of Chl-a is less in comparison to its
599 seasonal variability [Shi and Wang, 2022] implying the inter-species relationship to be at play in
600 shorter timescale with large and small phytoplankton dominating the SEAS [Shankar et al., 2019].
601 It is inferred that along with the physico-chemical parameters, the biology of ocean determines
602 the zooplankton-phytoplankton relationship and their biomass, respectively. This interdependency
603 of planktons and the physico-chemical drivers shows up as strong intra-seasonal and intra-annual
604 variability in zooplankton biomass as demonstrated in section 5.

605 The variability of zooplankton biomass in the intra-seasonal and lower period has strong impli-
606 cations on sampling. A servicing cruise along the EAS moorings takes about 12 to 15 days excluding
607 the time to and fro from port to first/last mooring [Chaudhuri et al., 2020, Aparna et al., 2022].
608 However, a sampling cruise dedicated to study the spatial variation of zooplankton [Madhupratap
609 et al., 1992, Smith et al., 1998, Wishner et al., 1998, Kidwai and Amjad, 2000], say for summer
610 monsoon may last a month or more with coarse sampling interval and hence fail to capture the
611 actual biomass within a season for a fair spatial comparison. One such occasion is a dip in zoo-
612 plankton biomass off Kollam because of intra-seasonal variability during August, 2019 (Fig. 10).
613 The resulting biomass is low even though the primary production in SEAS [Asha Devi et al., 2010,

614 Jyothibabu et al., 2010] is high and subsequent zooplankton biomass is supposed to be high. The
615 transient nature of variability also explains why Arabian sea paradox was seen as such. In northern
616 Arabian sea, the extended upwelling time leads to a longer and steady primary production, albeit
617 weaker than the southern counterpart [Madhupratap et al., 1996a, Smith and Madhupratap, 2005].
618 Provided the zooplankton-phytoplankton interaction is based on primary production, this may lead
619 to the zooplankton biomass to be consistent over season or longer i.e, weaker intraseasonal and
620 intra-annual variability, for example off Goa, June 2019 to September 2020, (Figs. 13 and 14) the
621 D215 remains at same depth, and this could be misinterpreted as constancy in zooplankton biomass
622 leading to paradoxical conclusions.

623 References

- 624 Anna-Karin Almén and Tobias Tamelander. Temperature-related timing of the spring bloom and match between
625 phytoplankton and zooplankton. *Marine Biology Research*, 16(8-9):674–682, 2020.
- 626 P Amol, D Shankar, V Fernando, A Mukherjee, SG Aparna, R Fernandes, GS Michael, ST Khalap, NP Satelkar,
627 Y Agarvadekar, et al. Observed intraseasonal and seasonal variability of the west india coastal current on the
628 continental slope. *Journal of Earth System Science*, 123(5):1045–1074, 2014.
- 629 P Amol, Suchandan Bemal, D Shankar, V Jain, V Thushara, V Vijith, and PN Vinayachandran. Modulation of
630 chlorophyll concentration by downwelling rossby waves during the winter monsoon in the southeastern arabian
631 sea. *Progress in Oceanography*, 186:102365, 2020.
- 632 SG Aparna, DV Desai, D Shankar, AC Anil, Shrikant Dora, and R Khedekar. Seasonal cycle of zooplankton standing
633 stock inferred from adcp backscatter measurements in the eastern arabian sea. *Progress in Oceanography*, 203:
634 102766, 2022.
- 635 C.R. Asha Devi, R. Jyothibabu, P. Sabu, Josia Jacob, H. Habeebrehman, M.P. Prabhakaran, K.J. Jayalakshmi, and
636 C.T. Achuthankutty. Seasonal variations and trophic ecology of microzooplankton in the southeastern arabian
637 sea. *Continental Shelf Research*, 30(9):1070–1084, 2010. ISSN 0278-4343. doi: <https://doi.org/10.1016/j.csr.2010.02.007>. URL <https://www.sciencedirect.com/science/article/pii/S0278434310000439>.
- 639 Carin J Ashjian, Sharon L Smith, Charles N Flagg, and Nasseer Idrisi. Distribution, annual cycle, and vertical
640 migration of acoustically derived biomass in the arabian sea during 1994–1995. *Deep Sea Research Part II:*
641 *Topical Studies in Oceanography*, 49(12):2377–2402, 2002.

- 642 K Banse and DC English. Geographical differences in seasonality of czcs-derived phytoplankton pigment in the
643 arabian sea for 1978–1986. *Deep Sea Research Part II: Topical Studies in Oceanography*, 47(7-8):1623–1677, 2000.
- 644 Karl Banse. Hydrography of the arabian sea shelf of india and pakistan and effects on demersal fishes. In *Deep sea*
645 *research and oceanographic Abstracts*, volume 15, pages 45–79. Elsevier, 1968.
- 646 Karl Banse. Zooplankton: pivotal role in the control of ocean production: I. biomass and production. *ICES Journal*
647 *of marine Science*, 52(3-4):265–277, 1995.
- 648 Richard T Barber, John Marra, Robert C Bidigare, Louis A Codispoti, David Halpern, Zackary Johnson, Mikel
649 Latasa, Ralf Goericke, and Sharon L Smith. Primary productivity and its regulation in the arabian sea during
650 1995. *Deep Sea Res. Part 2 Top. Stud. Oceanogr.*, 48(6-7):1127–1172, jan 2001.
- 651 WE Barraclough, RJ LeBrasseur, and OD Kennedy. Shallow scattering layer in the subarctic pacific ocean: detection
652 by high-frequency echo sounder. *Science*, 166(3905):611–613, 1969.
- 653 H. P. Batchelder, J. R. VanKeuren, R. D. Vaillancourt, and E. Swift. Spatial and temporal distributions of acoustically
654 estimated zooplankton biomass near the marine light-mixed layers station ($59^{\circ}30'N$, $21^{\circ}00'W$) in the north atlantic
655 in may 1991. *Journal of Geophysical Research: Oceans*, 100:6549–6563, 1995. doi: 10.1029/94jc00981.
- 656 John C Brock and Charles R McClain. Interannual variability in phytoplankton blooms observed in the northwestern
657 arabian sea during the southwest monsoon. *Journal of Geophysical Research: Oceans*, 97(C1):733–750, 1992.
- 658 John C Brock, Charles R McClain, Mark E Luther, and William W Hay. The phytoplankton bloom in the north-
659 western arabian sea during the southwest monsoon of 1979. *Journal of Geophysical Research: Oceans*, 96(C11):
660 20623–20642, 1991.
- 661 Abhisek Chatterjee, D Shankar, SSC Shenoi, GV Reddy, GS Michael, M Ravichandran, VV Gopalkrishna,
662 EP Rama Rao, TVS Udaya Bhaskar, and VN Sanjeevan. A new atlas of temperature and salinity for the north
663 indian ocean. *Journal of Earth System Science*, 121:559–593, 2012.
- 664 Anya Chaudhuri, D Shankar, SG Aparna, P Amol, V Fernando, A Kankonkar, GS Michael, NP Satelkar, ST Khalap,
665 AP Tari, et al. Observed variability of the west india coastal current on the continental slope from 2009–2018.
666 *Journal of Earth System Science*, 129(1):57, 2020.
- 667 Anya Chaudhuri, P Amol, D Shankar, S Mukhopadhyay, SG Aparna, V Fernando, and A Kankonkar. Observed
668 variability of the west india coastal current on the continental shelf from 2010–2017. *Journal of Earth System*
669 *Science*, 130:1–21, 2021.
- 670 Boris Cisewski, Volker H Strass, Monika Rhein, and Sören Krägesky. Seasonal variation of diel vertical migration
671 of zooplankton from adcp backscatter time series data in the lazarev sea, antarctica. *Deep Sea Research Part I:*
672 *Oceanographic Research Papers*, 57(1):78–94, 2010.
- 673 Kent L Deines. Backscatter estimation using broadband acoustic doppler current profilers. In *Proceedings of the*
674 *IEEE Sixth Working Conference on Current Measurement (Cat. No. 99CH36331)*, pages 249–253. IEEE, 1999.

- 675 A Edvardsen, D Slagstad, KS Tande, and P Jaccard. Assessing zooplankton advection in the barents sea using
676 underway measurements and modelling. *Fisheries Oceanography*, 12(2):61–74, 2003.
- 677 S Fielding, G Griffiths, and HSJ Roe. The biological validation of adcp acoustic backscatter through direct comparison
678 with net samples and model predictions based on acoustic-scattering models. *ICES Journal of Marine Science*,
679 61(2):184–200, 2004.
- 680 Charles N Flagg and Sharon L Smith. On the use of the acoustic doppler current profiler to measure zooplankton
681 abundance. *Deep Sea Research Part A. Oceanographic Research Papers*, 36(3):455–474, 1989.
- 682 Kevin D Friedland, Charles Stock, Kenneth F Drinkwater, Jason S Link, Robert T Leaf, Burton V Shank, Julie M
683 Rose, Cynthia H Pilskaln, and Michael J Fogarty. Pathways between primary production and fisheries yields of
684 large marine ecosystems. *PloS one*, 7(1):e28945, 2012.
- 685 H. E. García, R. A. Locarnini, T. P. Boyer, J. I. Antonov, A. V. Mishonov, O. K. Baranova, M. M. Zweng, J. R.
686 Reagan, and D. R. Johnson. Dissolved oxygen, apparent oxygen utilization, and oxygen saturation. *NOAA Atlas*
687 *NESDIS 75*, 3, 2014.
- 688 Charles H Greene, Peter H Wiebe, Chris Pelkie, Mark C Benfield, and Jacqueline M Popp. Three-dimensional
689 acoustic visualization of zooplankton patchiness. *Deep Sea Research Part II: Topical Studies in Oceanography*, 45
690 (7):1201–1217, 1998.
- 691 Charles F Greenlaw. Acoustical estimation of zooplankton populations 1. *Limnology and Oceanography*, 24(2):
692 226–242, 1979.
- 693 Davide Guerra, Katrin Schroeder, Mireno Borghini, Elisa Camatti, Marco Pansera, Anna Schroeder, Stefania
694 Sparnocchia, and Jacopo Chiggiato. Zooplankton diel vertical migration in the corsica channel (north-western
695 mediterranean sea) detected by a moored acoustic doppler current profiler. *Ocean Science*, 15(3):631–649, 2019.
- 696 James M Hamilton, Kate Collins, and Simon J Prinsenberg. Links between ocean properties, ice cover, and plankton
697 dynamics on interannual time scales in the canadian arctic archipelago. *Journal of Geophysical Research: Oceans*,
698 118(10):5625–5639, 2013.
- 699 Graeme C Hays. A review of the adaptive significance and ecosystem consequences of zooplankton diel vertical
700 migrations. In *Migrations and Dispersal of Marine Organisms: Proceedings of the 37 th European Marine Biology*
701 *Symposium held in Reykjavík, Iceland, 5–9 August 2002*, pages 163–170. Springer, 2003.
- 702 PJ Herring, MJR Fasham, AR Weeks, JCP Hemmings, HSJ Roe, PR Pugh, S Holley, NA Crisp, and MV Angel.
703 Across-slope relations between the biological populations, the euphotic zone and the oxygen minimum layer off
704 the coast of oman during the southwest monsoon (august, 1994). *Progress in Oceanography*, 41(1):69–109, 1998.
- 705 Karen J Heywood, S Scrope-Howe, and ED Barton. Estimation of zooplankton abundance from shipborne adcp
706 backscatter. *Deep Sea Research Part A. Oceanographic Research Papers*, 38(6):677–691, 1991.

- 707 Laura Hobbs, Neil S Banas, Jonathan H Cohen, Finlo R Cottier, Jørgen Berge, and Øystein Varpe. A marine
708 zooplankton community vertically structured by light across diel to interannual timescales. *Biology Letters*, 17(2):
709 20200810, 2021.
- 710 Raleigh R Hood, Lynnath E Beckley, and Jerry D Wiggert. Biogeochemical and ecological impacts of boundary
711 currents in the indian ocean. *Progress in Oceanography*, 156:290–325, 2017.
- 712 Ryuichiro Inoue, Minoru Kitamura, and Tetsuichi Fujiki. Diel vertical migration of zooplankton at the s 1 biogeo-
713 chemical mooring revealed from acoustic backscattering strength. *Journal of Geophysical Research: Oceans*, 121
714 (2):1031–1050, 2016.
- 715 D. A. Jayakumar, Christopher A. Francis, S.W.A. Naqvi, and Bess B. Ward. Diversity of nitrite reductase genes
716 (*nirs*) in the denitrifying water column of the coastal arabian sea. *Aquatic Microbial Ecology*, 2004. doi: 10.3354/
717 ame034069.
- 718 Songnian Jiang, Tommy D Dickey, Deborah K Steinberg, and Laurence P Madin. Temporal variability of zooplankton
719 biomass from adcp backscatter time series data at the bermuda testbed mooring site. *Deep Sea Research Part I:*
720 *Oceanographic Research Papers*, 54(4):608–636, 2007.
- 721 R Jyothibabu, NV Madhu, H Habeebrehman, KV Jayalakshmy, KKC Nair, and CT Achuthankutty. Re-evaluation
722 of ‘paradox of mesozooplankton’ in the eastern arabian sea based on ship and satellite observations. *Journal of*
723 *Marine Systems*, 81(3):235–251, 2010.
- 724 Myounghee Kang, Sunyoung Oh, Wooseok Oh, Dong-Jin Kang, SungHyun Nam, and Kyounghoon Lee. Acoustic
725 characterization of fish and macroplankton communities in the seychelles-chagos thermocline ridge of the southwest
726 indian ocean. *Deep Sea Research Part II: Topical Studies in Oceanography*, 213:105356, 2024.
- 727 Madhavan Girijakumari Keerthi, Matthieu Lengaigne, Marina Levy, Jerome Vialard, Vallivattathillam Parvathi,
728 Clément de Boyer Montégut, Christian Ethé, Olivier Aumont, Iyyappan Suresh, Valiya Parambil Akhil, et al.
729 Physical control of interannual variations of the winter chlorophyll bloom in the northern arabian sea. *Bioge-
730 sciences*, 14(15):3615–3632, 2017.
- 731 Punam A Khandagale, Vaibhav D Mhatre, and Sujitha Thomas. Seasonal and spatial variability of zooplankton
732 diversity in north eastern arabian sea along the maharashtra coast. *Journal of the Marine Biological Association*
733 *of India*, 64(1):25–32, 2022.
- 734 S Kidwai and S Amjad. Zooplankton: pre-southwest and northeast monsoons of 1993 to 1994, from the north arabian
735 sea. *Mar. Biol.*, 136(3):561–571, apr 2000.
- 736 S. Prasanna Kumar, M. Madhupratap, M. Dileep Kumar, Mangesh Gauns, P.M. Muraleedharan, V. V. S. S. Sarma,
737 and Sílvia Naves de Souza. Physical control of primary productivity on a seasonal scale in central and eastern
738 arabian sea. *Journal of Earth System Science*, 2000. doi: 10.1007/bf02708331.

- 739 Corinne Le Qu, Robbie M Andrew, Josep G Canadell, Stephen Sitch, Jan Ivar Korsbakken, Glen P Peters, Andrew C
740 Manning, Thomas A Boden, Pieter P Tans, Richard A Houghton, et al. Global carbon budget 2016. *Earth System*
741 *Science Data*, 8(2):605–649, 2016.
- 742 Marina Lévy, D Shankar, J-M André, SSC Shenoi, Fabien Durand, and Clément de Boyer Montégut. Basin-wide
743 seasonal evolution of the Indian Ocean's phytoplankton blooms. *Journal of Geophysical Research: Oceans*, 112
744 (C12), 2007.
- 745 M Li, A Gargett, and K Denman. What determines seasonal and interannual variability of phytoplankton and
746 zooplankton in strongly estuarine systems? *Estuarine, Coastal and Shelf Science*, 50(4):467–488, 2000.
- 747 Yanliang Liu, Jingsong Guo, Yuhuan Xue, Chalermrat Sangmanee, Huiwu Wang, Chang Zhao, Somkiat Khokiat-
748 tiwong, and Weidong Yu. Seasonal variation in diel vertical migration of zooplankton and microneuston in the
749 Andaman Sea observed by a moored ADCP. *Deep Sea Research Part I: Oceanographic Research Papers*, 179:103663,
750 2022.
- 751 Alan R Longhurst and Warren S Wooster. Abundance of oil sardine (*Sardinella longiceps*) and upwelling on the
752 southwest coast of India. *Can. J. Fish. Aquat. Sci.*, 47(12):2407–2419, dec 1990.
- 753 M Madhupratap, P Haridas, Neelam Ramaiah, and CT Achuthankutty. Zooplankton of the southwest coast of India:
754 abundance, composition, temporal and spatial variability in 1987. 1992.
- 755 M Madhupratap, TC Gopalakrishnan, P Haridas, KKC Nair, PN Aravindakshan, G Padmavati, and Shiney Paul.
756 Lack of seasonal and geographic variation in mesozooplankton biomass in the Arabian Sea and its structure in the
757 mixed layer. *Current science. Bangalore*, 71(11):863–868, 1996a.
- 758 M Madhupratap, S Prasanna Kumar, PMA Bhattachari, M Dileep Kumar, S Raghukumar, KKC Nair, and N Rama-
759 iah. Mechanism of the biological response to winter cooling in the northeastern Arabian Sea. *Nature*, 384(6609):
760 549–552, 1996b.
- 761 M Madhupratap, TC Gopalakrishnan, P Haridas, and KKC Nair. Mesozooplankton biomass, composition and
762 distribution in the Arabian Sea during the fall intermonsoon: implications of oxygen gradients. *Deep Sea Research*
763 *Part II: Topical Studies in Oceanography*, 48(6–7):1345–1368, 2001.
- 764 PA Maheswaran, G Rajesh, C Revichandran, and KKC Nair. Upwelling and associated hydrography along the west
765 coast of India during southwest monsoon, 1999. 2000.
- 766 John Marra and Richard T. Barber. Primary productivity in the Arabian Sea: A synthesis of JGOFS data. *Progress*
767 *in Oceanography*, 65(2):159–175, 2005. ISSN 0079-6611. doi: <https://doi.org/10.1016/j.pocean.2005.03.004>. URL
768 <https://www.sciencedirect.com/science/article/pii/S007966110500042X>. The Arabian Sea of the 1990s: New
769 Biogeochemical Understanding.
- 770 JP McCreary, Raghu Murtugudde, Jerome Vialard, PN Vinayachandran, Jerry D Wiggert, Raleigh R Hood,
771 D Shankar, and S Shetye. Biophysical processes in the Indian Ocean. *Indian Ocean biogeochemical processes*
772 and ecological variability

- 773 Julian P McCreary Jr, Pijush K Kundu, and Robert L Molinari. A numerical investigation of dynamics, thermodynamics and mixed-layer processes in the indian ocean. *Progress in Oceanography*, 31(3):181–244, 1993.
- 775 Donald C McNaught. Acoustical determination of zooplankton distribution. In *Proc. 11th Conf. Great lakes Res.*,
776 pages 76–84, 1968.
- 777 John M Morrison, LA Codispoti, S Gaurin, Burton Jones, V Manghnani, and Z Zheng. Seasonal variation of
778 hydrographic and nutrient fields during the us jgofs arabian sea process study. *Deep Sea Research Part II: Topical
779 Studies in Oceanography*, 45(10-11):2053–2101, 1998.
- 780 A Mukherjee, D Shankar, V Fernando, P Amol, SG Aparna, R Fernandes, GS Michael, ST Khalap, NP Satelkar,
781 Y Agarvadekar, et al. Observed seasonal and intraseasonal variability of the east india coastal current on the
782 continental slope. *Journal of Earth System Science*, 123(6):1197–1232, 2014.
- 783 S Mukhopadhyay, D Shankar, SG Aparna, A Mukherjee, V Fernando, A Kankonkar, S Khalap, NP Satelkar,
784 MG Gaonkar, AP Tari, et al. Observed variability of the east india coastal current on the continental slope
785 during 2009–2018. *Journal of Earth System Science*, 129:1–22, 2020.
- 786 Jerry Mullison. Backscatter estimation using broadband acoustic doppler current profilers-updated. In *Proceedings
787 of the ASCE Hydraulic Measurements & Experimental Methods Conference, Durham, NH, USA*, pages 9–12,
788 2017.
- 789 KKC Nair, M Madhupratap, TC Gopalakrishnan, P Haridas, and Mangesh Gauns. The arabian sea: physical
790 environment, zooplankton and myctophid abundance. 1999.
- 791 PV Nair. Primary productivity in the indian seas. *CMFRI Bulletin*, 22:1–63, 1970.
- 792 D Nethery and D Shankar. Vertical propagation of baroclinic kelvin waves along the west coast of india. *J. Earth
793 Syst. Sci.*, 116(4):331–339, aug 2007.
- 794 Lingyun Nie, Jianchao Li, Hao Wu, Wenchao Zhang, Yongjun Tian, Yang Liu, Peng Sun, Zhenjiang Ye, Shuyang
795 Ma, and Qinfeng Gao. The influence of ocean processes on fine-scale changes in the yellow sea cold water mass
796 boundary area structure based on acoustic observations. *Remote Sensing*, 15(17):4272, 2023.
- 797 MD Ohman and H-J Hirche. Density-dependent mortality in an oceanic copepod population. *Nature*, 412(6847):
798 638–641, 2001.
- 799 G Padmavati, P Haridas, KKC Nair, TC Gopalakrishnan, P Shiney, and M Madhupratap. Vertical distribution of
800 mesozooplankton in the central and eastern arabian sea during the winter monsoon. *Journal of Plankton Research*,
801 20(2):343–354, 1998.
- 802 MR Patil, CP Ramamirtham, P Udaya Varma, and CP Nair. Hydrography of the west coast of india during the
803 pre-monsoon period of the year 1962. *Journal of marine biological association of India*, 6(1):151–164, 1964.

- 804 Richard Edward Pieper. *A study of the relationship between zooplankton and high-frequency scattering of underwater*
805 *sound*. PhD thesis, University of British Columbia, 1971.
- 806 SA Piontkovski, R Williams, and TA Melnik. Spatial heterogeneity, biomass and size structure of plankton of the
807 indian ocean: some general trends. *Marine ecology progress series*, pages 219–227, 1995.
- 808 Emmanuel Potiris, Constantin Frangoulis, Alkiviadis Kalampokis, Manolis Ntoumas, Manos Pettas, George Peti-
809 hakis, and Vassilis Zervakis. Acoustic doppler current profiler observations of migration patterns of zooplankton
810 in the cretan sea. *Ocean Science*, 14(4):783–800, 2018.
- 811 SZ Qasim. Biological productivity of the indian ocean. 1977.
- 812 CP Ramamirtham and AVS Murty. Hydrography of the west coast of india during the pre-monsoon period of the
813 year 1962—part 2: in and offshore waters of the konkan and malabar coasts. *Journal of the Marine Biological*
814 *Association of India*, 7(1):150–168, 1965.
- 815 S Ramamurthy. Studies on the plankton of the north kanara coast in relation to the pelagic fishery. *Journal of*
816 *Marine Biological Association of India*, 7(1):127–149, 1965.
- 817 Mehbuba Rehim and Mudassar Imran. Dynamical analysis of a delay model of phytoplankton–zooplankton interac-
818 tion. *Applied Mathematical Modelling*, 36(2):638–647, 2012.
- 819 T. P. Rippeth and J. H. Simpson. Diurnal signals in vertical motions on the hebridean shelf. *Limnology and*
820 *Oceanography*, 43:1690–1696, 1998. doi: 10.4319/lo.1998.43.7.1690.
- 821 John H Ryther, John R Hall, Allan K Pease, Andrew Bakun, and Mark M Jones. Primary organic production in
822 relation to the chemistry and hydrography of the western indian ocean 1. *Limnology and Oceanography*, 11(3):
823 371–380, 1966.
- 824 D Sameoto and S Paulowich. The use of 120 khz sonar in zooplankton studies. In *OCEANS'77 Conference Record*,
825 pages 523–528. IEEE, 1977.
- 826 VVSS Sarma, TVS Udaya Bhaskar, J Pavan Kumar, and Kunal Chakraborty. Potential mechanisms responsible for
827 occurrence of core oxygen minimum zone in the north-eastern arabian sea. *Deep Sea Research Part I: Oceanographic*
828 *Research Papers*, 165:103393, 2020.
- 829 Friedrich A. Schott and Julian P. McCreary. The monsoon circulation of the indian ocean. *Progress in Oceanography*,
830 51(1):1–123, 2001. ISSN 0079-6611. doi: [https://doi.org/10.1016/S0079-6611\(01\)00083-0](https://doi.org/10.1016/S0079-6611(01)00083-0). URL <https://www.sciencedirect.com/science/article/pii/S0079661101000830>.
- 832 D Shankar and SR Shetye. On the dynamics of the lakshadweep high and low in the southeastern arabian sea.
833 *Journal of Geophysical Research: Oceans*, 102(C6):12551–12562, 1997.
- 834 D Shankar, R Remya, PN Vinayachandran, Abhisek Chatterjee, and Ambica Behera. Inhibition of mixed-layer
835 deepening during winter in the northeastern arabian sea by the west india coastal current. *Climate Dynamics*,
836 47:1049–1072, 2016.

- 837 D Shankar, R Remya, AC Anil, and V Vijith. Role of physical processes in determining the nature of fisheries in the
838 eastern arabian sea. *Progress in Oceanography*, 172:124–158, 2019.
- 839 SR Shetye and AD Gouveia. Coastal circulation in the north indian ocean: Coastal segment (14, sw). John Wiley
840 and Sons, New York, USA, 1998.
- 841 SR Shetye, AD Gouveia, SSC Shenoi, D Sundar, GS Michael, AM Almeida, and K Santanam. Hydrography and
842 circulation off the west coast of india during the southwest monsoon 1987. 1990.
- 843 SR Shetye, AD Gouveia, SSC Shenoi, GS Michael, D Sundar, AM Almeida, and K Santanam. The coastal current
844 off western india during the northeast monsoon. *Deep Sea Research Part A. Oceanographic Research Papers*, 38
845 (12):1517–1529, 1991.
- 846 SR Shetye, AD Gouveia, and SSC Shenoi. Does winter cooling lead to the subsurface salinity minimum off saurashtra,
847 india? *Oceanography of the Indian Ocean*, pages 617–625, 1992.
- 848 Wei Shi and Menghua Wang. Phytoplankton biomass dynamics in the arabian sea from viirs observations. *Journal
849 of Marine Systems*, 227:103670, 2022.
- 850 Wei Shi, John M Morrison, Emanuele Böhm, and Vijayakumar Manghnani. Remotely sensed features in the us jgofs
851 arabian sea process study. *Deep Sea Research Part II: Topical Studies in Oceanography*, 46(8-9):1551–1575, 1999.
- 852 Greg M Silsbe, Michael J Behrenfeld, Kimberly H Halsey, Allen J Milligan, and Toby K Westberry. The cafe model:
853 A net production model for global ocean phytoplankton. *Global Biogeochemical Cycles*, 30(12):1756–1777, 2016.
- 854 Houssem Smeti, Marc Pagano, Christophe Menkes, Anne Lebourges-Dhaussy, Brian PV Hunt, Valerie Allain, Martine
855 Rodier, Florian De Boissieu, Elodie Kestenare, and Cherif Sammari. Spatial and temporal variability of zooplankton
856 off n ew c aledonia (s outhwestern p acific) from acoustics and net measurements. *Journal of Geophysical
857 Research: Oceans*, 120(4):2676–2700, 2015.
- 858 Sharon Smith, Michael Roman, Irina Prusova, Karen Wishner, Marcia Gowing, LA Codispoti, Richard Barber, John
859 Marra, and Charles Flagg. Seasonal response of zooplankton to monsoonal reversals in the arabian sea. *Deep Sea
860 Research Part II: Topical Studies in Oceanography*, 45(10-11):2369–2403, 1998.
- 861 SL Smith and M Madhupratap. Mesozooplankton of the arabian sea: patterns influenced by seasons, upwelling, and
862 oxygen concentrations. *Progress in Oceanography*, 65(2-4):214–239, 2005.
- 863 Patnaik Sreenivas, KVKRK Patnaik, and KVSR Prasad. Monthly variability of mixed layer over arabian sea using
864 argo data. *Marine Geodesy*, 31(1):17–38, 2008.
- 865 R Subrahmanyam. Studies on the phytoplankton of the west coast of india: Part ii. physical and chemical factors
866 influencing the production of phytoplankton, with remarks on the cycle of nutrients and on the relationship of
867 the phosphate-content to fish landings. In *Proceedings/Indian Academy of Sciences*, volume 50, pages 189–252.
868 Springer, 1959.

- 869 R Subrahmanyam and AH Sarma. Studies on the phytoplankton of the west coast of india. part iii. seasonal variation
870 of the phytoplankters and environmental factors. *Indian Journal of Fisheries*, 7(2):307–336, 1960.
- 871 V. Sudheesh, G.V.M. Gupta, Yudhishtir Reddy, Kausar F. Bepari, N.V.H.K. Chari, C.K. Sherin, S.S. Shaju, Ch.V.
872 Ramu, and Anil Kumar Vijayan. Oxygen minimum zone along the eastern arabian sea: Intra-annual varia-
873 tion and dynamics based on ship-borne studies. *Progress in Oceanography*, 201:102742, 2022. ISSN 0079-6611.
874 doi: <https://doi.org/10.1016/j.pocean.2022.102742>. URL <https://www.sciencedirect.com/science/article/pii/S0079661122000040>.
- 875 Laura Ursella, Vanessa Cardin, Mirna Batistić, Rade Garić, and Miroslav Gačić. Evidence of zooplankton vertical
876 migration from continuous southern adriatic buoy current-meter records. *Progress in oceanography*, 167:78–96,
877 2018.
- 878 Laura Ursella, Sara Pensieri, Enric Pallàs-Sanz, Sharon Z Herzka, Roberto Bozzano, Miguel Tenreiro, Vanessa Cardin,
879 Julio Candela, and Julio Sheinbaum. Diel, lunar and seasonal vertical migration in the deep western gulf of mexico
880 evidenced from a long-term data series of acoustic backscatter. *Progress in Oceanography*, 195:102562, 2021.
- 881 V Vijith, PN Vinayachandran, V Thushara, P Amol, D Shankar, and AC Anil. Consequences of inhibition of mixed-
882 layer deepening by the west india coastal current for winter phytoplankton bloom in the northeastern arabian sea.
883 *Journal of Geophysical Research: Oceans*, 121(9):6583–6603, 2016.
- 884 Peter H Wiebe, Charles H Greene, Timothy K Stanton, and Janusz Burczynski. Sound scattering by live zooplankton
885 and micronekton: empirical studies with a dual-beam acoustical system. *The Journal of the Acoustical Society of
886 America*, 88(5):2346–2360, 1990.
- 887 Monika Winder and Daniel E Schindler. Climatic effects on the phenology of lake processes. *Global change biology*,
888 10(11):1844–1856, 2004.
- 889 Karen F Wishner, Marcia M Gowing, and Celia Gelfman. Mesozooplankton biomass in the upper 1000 m in the
890 arabian sea: overall seasonal and geographic patterns, and relationship to oxygen gradients. *Deep Sea Research
891 Part II: Topical Studies in Oceanography*, 45(10-11):2405–2432, 1998.

Table 1: ADCP deployment details at the locations. The temporal resolution is 1 hour, bin size(vertical resolution) 4 m. All ADCPs are operated at 153.3 kHz. The moorings are at a water column depth of 950 – 1200 m on the continental slope and are serviced on yearly basis according to ship availability. The 6th column consists of Reference echo intensity (Er) for each beam, while the 7th column contains the corresponding RSSI conversion factor [Deines, 1999].

Station (Position; $^{\circ}$ E, $^{\circ}$ N)	Date		Depth			
	Deployment	Recovery	Ocean	ADCP	Er	Kc
Okha (67.47, 22.26)	01/10/2018	01/12/2019	996	118	37 , 37 , 37 , 36	0.42 , 0.44 , 0.42 , 0.43
	01/12/2019	04/12/2020	1166	312	39 , 36 , 38 , 36	0.42 , 0.44 , 0.42 , 0.43
	04/12/2020	08/03/2022	1021	144	41 , 37 , 38 , 37	0.42 , 0.44 , 0.42 , 0.43
	08/03/2022	01/01/2023	1019	142	37 , 38 , 39 , 36	0.42 , 0.44 , 0.42 , 0.43
Mumbai (69.24, 20.01)	09/11/2017	29/09/2018	1025	150	36 , 34 , 39 , 42	0.40 , 0.40 , 0.40 , 0.40
	29/09/2018	29/11/2019	1122	125	35 , 36 , 39 , 42	0.40 , 0.40 , 0.40 , 0.40
	29/11/2019	02/12/2020	1143	164	37 , 34 , 39 , 43	0.40 , 0.40 , 0.40 , 0.40
	02/12/2020	06/03/2022	1125	142	36 , 34 , 39 , 42	0.40 , 0.40 , 0.40 , 0.40
	07/03/2022	02/01/2023	1103	158	37 , 34 , 40 , 43	0.40 , 0.40 , 0.40 , 0.40
Jaigarh (71.12, 17.53)	27/10/2017	27/09/2018	1039	198	32 , 35 , 33 , 32	0.45 , 0.45 , 0.45 , 0.45
	27/09/2018	30/10/2019	1032	164	32 , 35 , 33 , 31	0.45 , 0.45 , 0.45 , 0.45
	03/11/2019	30/11/2020	1142	264	32 , 36 , 33 , 32	0.45 , 0.45 , 0.45 , 0.45
	30/11/2020	05/03/2022	1099	119	33 , 36 , 34 , 32	0.45 , 0.45 , 0.45 , 0.45
Goa (72.74, 15.17)	03/10/2017	25/09/2018	1000	174	35 , 37 , 34 , 35	0.44 , 0.44 , 0.40 , 0.41
	25/09/2018	16/10/2019	969	145	38 , 36 , 36 , 34	0.44 , 0.44 , 0.40 , 0.41
	16/10/2019	29/11/2020	966	143	44 , 38 , 36 , 43	0.44 , 0.44 , 0.40 , 0.41
	29/11/2020	03/03/2022	985	157	35 , 40 , 35 , 38	0.44 , 0.44 , 0.40 , 0.41
	03/03/2022	05/01/2023	984	159	35 , 38 , 35 , 34	0.44 , 0.44 , 0.40 , 0.41
Udupi (74.04, 12.5)	05/10/2017	06/10/2018	1028	176	44 , 46 , 29 , 35	0.45 , 0.45 , 0.45 , 0.45
	06/10/2018	18/10/2019	1027	179	32 , 38 , 30 , 36	0.45 , 0.45 , 0.45 , 0.45
	18/10/2019	11/12/2020	1018	168	33 , 37 , 31 , 38	0.45 , 0.45 , 0.45 , 0.45
	11/03/2022	06/01/2023	1036	155	31 , 32 , 32 , 33	0.45 , 0.45 , 0.45 , 0.45
Kollam (75.44, 9.05)	07/10/2017	08/10/2018	1174	200	43 , 55 , 45 , 43	0.49 , 0.50 , 0.49 , 0.50
	08/10/2018	20/10/2019	1160	123	49 , 62 , 46 , 46	0.49 , 0.50 , 0.49 , 0.50
	20/10/2019	13/12/2020	1209	176	52 , 61 , 54 , 55	0.49 , 0.50 , 0.49 , 0.50
	13/12/2020	13/03/2022	1129	91	49 , 51 , 46 , 47	0.49 , 0.50 , 0.49 , 0.50
	13/03/2022	08/01/2023	1149	164	41 , 48 , 43 , 41	0.49 , 0.50 , 0.49 , 0.50
Kanyakumari (77.39, 6.96)	16/11/2016	08/10/2017	1096	252	37 , 36 , 37 , 37	0.42 , 0.44 , 0.42 , 0.43
	08/10/2017	10/10/2018	1055	181	32 , 34 , 38 , 35	0.45 , 0.45 , 0.45 , 0.45
	10/10/2018	22/10/2019	1075	180	36 , 34 , 39 , 36	0.45 , 0.45 , 0.45 , 0.45
	22/10/2019	14/12/2020	1060	167	33 , 35 , 36 , 35	0.45 , 0.45 , 0.45 , 0.45
	14/12/2020	14/03/2022	1184	287	34 , 36 , 36 , 35	0.45 , 0.45 , 0.45 , 0.45

Table 2:

Volumetric samples of zooplankton of various stations. The sampling depth range is standardised for later years for bin range of 0–25m, 25–50m, 50–75m, 75–100m, 100–150m. The abbreviations are in the following manner: Okha (O), Mumbai (M), Jaigarh (J), Goa (G), Udupi (U), Kollam (K), Kanyakumari (KK); The number tags corresponds to particular cruise of a station.

Sample number	Tag	Lat($^{\circ}$ N)	Lon($^{\circ}$ E)	Date	Time (IST)	Sampling depth range (m)
1-3	G1	15.18	72.79	25 Sep 18	452	50–25, 100–50, 150–100
4-6	G2	15.16	72.71	25 Sep 18	2108	50–25, 100–50, 150–100
7-10	G2	15.16	72.71	25 Sep 18	2137	40–20, 60–40, 80–60, 100–80
11-14	J1			26 Sep 18	2000	40–20, 60–40, 80–60, 100–80
15-17	J2			27 Sep 18	2000	50–25, 100–50, 150–100
18-21	J2			27 Sep 18	2100	40–20, 60–40, 80–60, 100–80
22-25	M1	20	69.19	28 Sep 18	2135	40–20, 60–40, 80–60, 100–80
26-27	M1	20	69.19	28 Sep 18	2205	50–25, 100–50
28-29	M2	20.01	69.2	29 Sep 18	2035	50–25, 100–50
30-33	M2	20.01	69.2	29 Sep 18	2057	40–20, 60–40, 80–60, 100–80
34-37	U1			5 Oct 18	2000	40–20, 60–40, 80–60, 100–80
38-40	U1			5 Oct 18	2100	50–25, 100–50, 150–100
41-43	U2			6 Oct 18	2000	50–25, 100–50, 150–100
44-47	U2			6 Oct 18	2100	40–20, 60–40, 80–60, 100–80
48-51	K1	9.06	75.42	8 Oct 18	421	40–20, 60–40, 80–60, 100–80
52-54	K1	9.06	75.42	8 Oct 18	449	50–25, 100–50, 150–100
55-56	K2	9.04	75.4	8 Oct 18	2027	50–25, 100–50
57-60	K2	9.04	75.4	8 Oct 18	2045	40–20, 60–40, 80–60, 100–80
61-64	G2	15.16	72.74	16 Oct 19	829	50–25, 75–50, 100–75, 150–100
65-67	G3	15.16	72.74	16 Oct 19	1812	50–25, 75–50, 100–75
68-70	K2	9.02	75.42	20 Oct 19	840	50–25, 75–50, 100–75
71-74	K3	9.04	75.43	20 Oct 19	1934	50–25, 75–50, 100–75, 150–100
75-78	KK1			22 Oct 19	742	50–25, 75–50, 100–75, 150–100
79-82	KK2			22 Oct 19	1925	50–25, 75–50, 100–75, 150–100
83-86	J1			30 Oct 19	324	50–25, 75–50, 100–75, 150–100
87-89	J2			4 Nov 19	946	75–50, 100–75, 150–100
90-92	M2	19.98	69.22	29 Nov 19	1434	50–25, 75–50, 100–75
93-96	M3	20.01	69.23	30 Nov 19	958	50–25, 75–50, 100–75, 150–100
97-100	O1	22.24	67.49	1 Dec 19	937	50–25, 75–50, 100–75, 150–100
101	O2	22.25	67.46	1 Dec 19	1957	150–100
102-105	G3	15.68	73.22	28 Nov 20	930	50–25, 75–50, 100–75, 150–100
105-108	G4	15.32	73.22	29 Nov 20	1558	50–25, 75–50, 100–75, 150–100
108-110	J2	17.85	71.21	30 Nov 20	1458	75–50, 100–75, 150–100
111-114	J3	17.91	71.21	1 Dec 20	1052	50–25, 75–50, 100–75, 150–100
115-118	M4	20.03	69.38	2 Dec 20	2016	50–25, 75–50, 100–75, 150–100
119-00	O2	22.41	67.8	4 Dec 20	953	150–100
120-123	O3	22.41	67.79	4 Dec 20	2011	50–25, 75–50, 100–75, 150–100
124-127	K3	9.11	75.72	12 Dec 20	2335	50–25, 75–50, 100–75, 150–100
128-131	K4	9.06	75.74	13 Dec 20	1507	50–25, 75–50, 100–75, 150–100
132-134	KK1	7.62	77.63	14 Dec 20	1226	50–25, 75–50
135-138	KK2	7.62	77.63	14 Dec 20	2047	50–25, 75–50, 100–75, 150–100
139-142	G4	15.32	73.21	3 Mar 22	823	50–25, 75–50, 100–75, 150–100
143-146	G5	15.68	73.21	4 Mar 22	1030	50–25, 75–50, 100–75, 150–100
147-150	M5	19.99	69.23	7 Mar 22	957	50–25, 75–50, 100–75, 150–100
151-154	O3	22.24	67.5	8 Mar 22	806	50–25, 75–50, 100–75, 150–100
155-158	U3	12.5	74.04	12 Mar 22	1156	50–25, 75–50, 100–75, 150–100
159-160	K4	9.04	75.42	13 Mar 22	1027	50–25, 75–50, 100–75
161-164	KK3	6.97	77.4	15 Mar 22	1220	50–25, 75–50, 100–75, 150–100

Table 3:
The mean, standard deviation at 40 and 104 m of zooplankton biomass ($mg\ m^{-3}$), standard deviation of zooplankton standing stock ($mg\ m^{-2}$) and chlorophyll ($mg\ m^{-3}$) at 7 mooring sites are tabulated.

	Biomass (40 m)		Biomass (100 m)		Standard deviation	
	Mean	std	Mean	std	ZSS ($gm\ m^{-2}$)	Chl ($mg\ m^{-3}$)
Okha	230.42	22.84	151.68	25.58	1.93	0.25
Mumbai	272.86	34.95	182.24	30.34	2.9	0.13
Jaigarh	278.45	36.52	182.96	48.89	3.24	0.05
Goa	235.22	30.34	163.02	36.54	2.24	0.15
Udupi	247.81	34.37	169.37	38.8	2	0.55
Kollam	272.56	54.94	198.89	50.08	1.25	0.68
KanyaKumari	207.07	30.42	167.63	20.89	0.67	0.51

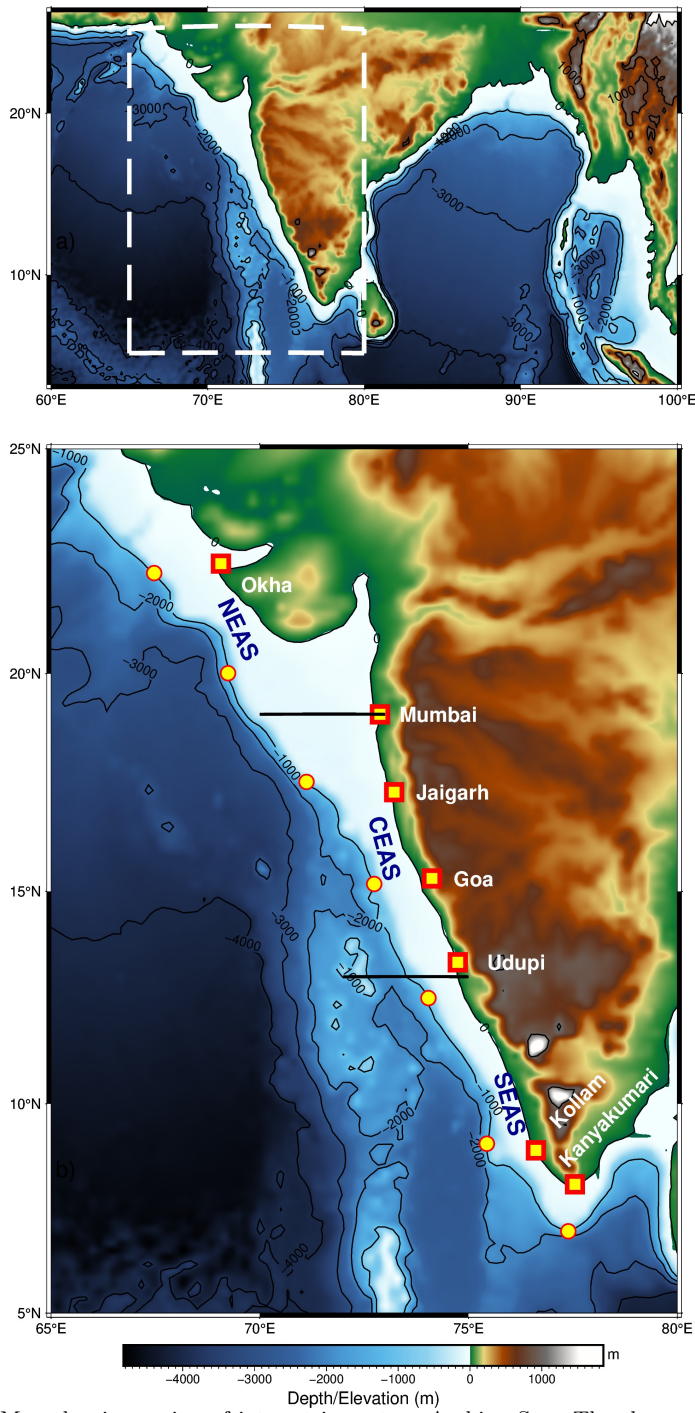


Figure 1: Map showing region of interest in eastern Arabian Sea. The slope moorings are deployed at ~ 1000 m depth as shown in the bathymetry contour. Note the increase in shelf width as we go poleward along the coast. The mooring sites off Okha and Mumbai are in Northern EAS; Jaigarh and Goa in Central EAS while Kollam and Kanyakumari are at Southern EAS. Udupi is situated at the transition zone of Central and Southern EAS.

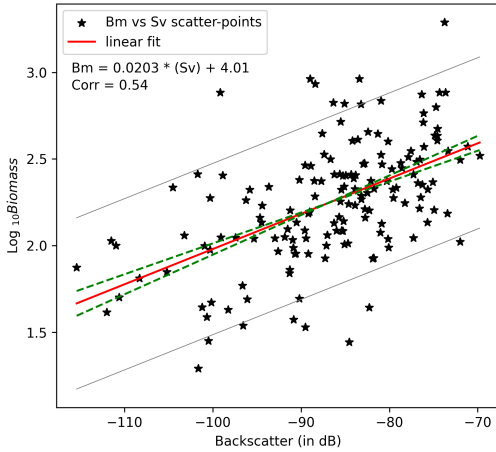


Figure 2: The linear fit line of Biomass (\log_{10} scale) and backscattering strength (in dB). The linear fit line is within the error range of previous result of [Aparna et al., 2022] (contained 67 data points) onto which latest zooplankton volumetric sample data (159 data points) is appended. The regression equation is $y = (0.02 \pm 0.0025)x + (4.0144 \pm 0.2198)$ and correlation value of 0.54. The dashed green lines denote error range of plausible slope and intercept. The first standard deviation of $\log_{10}(\text{Biomass})$ is ± 0.49 , which results in the backscatter range of 48.58 dB encompassing the entire backscatter range. It signifies the robustness of zooplankton biomass dependency on ADCP measured backscattering strength.

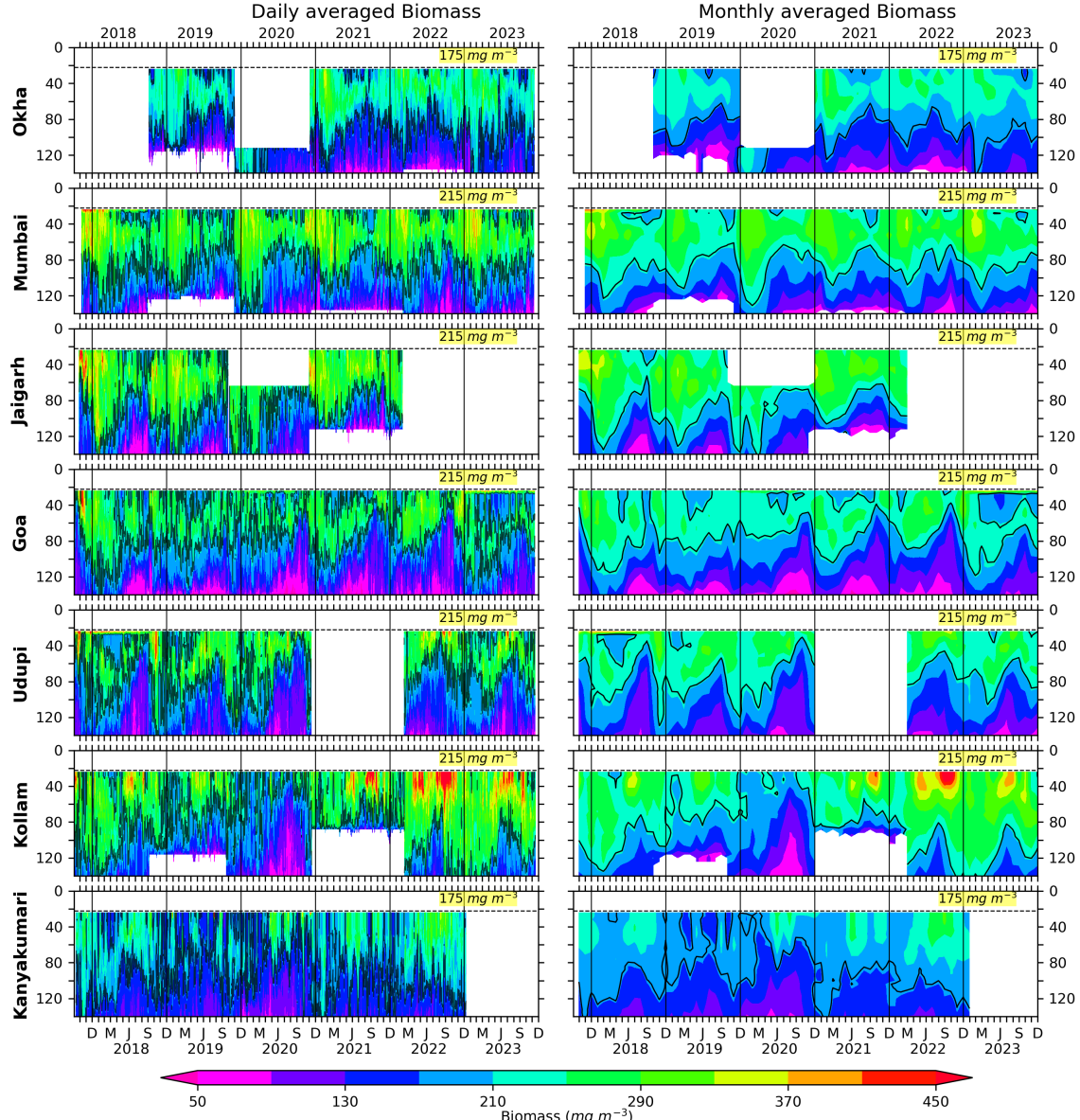


Figure 3: The Daily and monthly averaged biomass for EAS moorings, north (top) to south (bottom). The black contours are marking of 175 mg m^{-3} biomass for Okha and Kanyakumari; 215 mg m^{-3} for Mumbai, Goa and Kollam. The biomass contours are distinct and different based on the physico-chemical parameters and the one that best explains seasonality at respective location. The top 10 % of data is discarded due to echo noise. The dashed line at 22 m marks the top-depth of first bin i.e., 24 m.

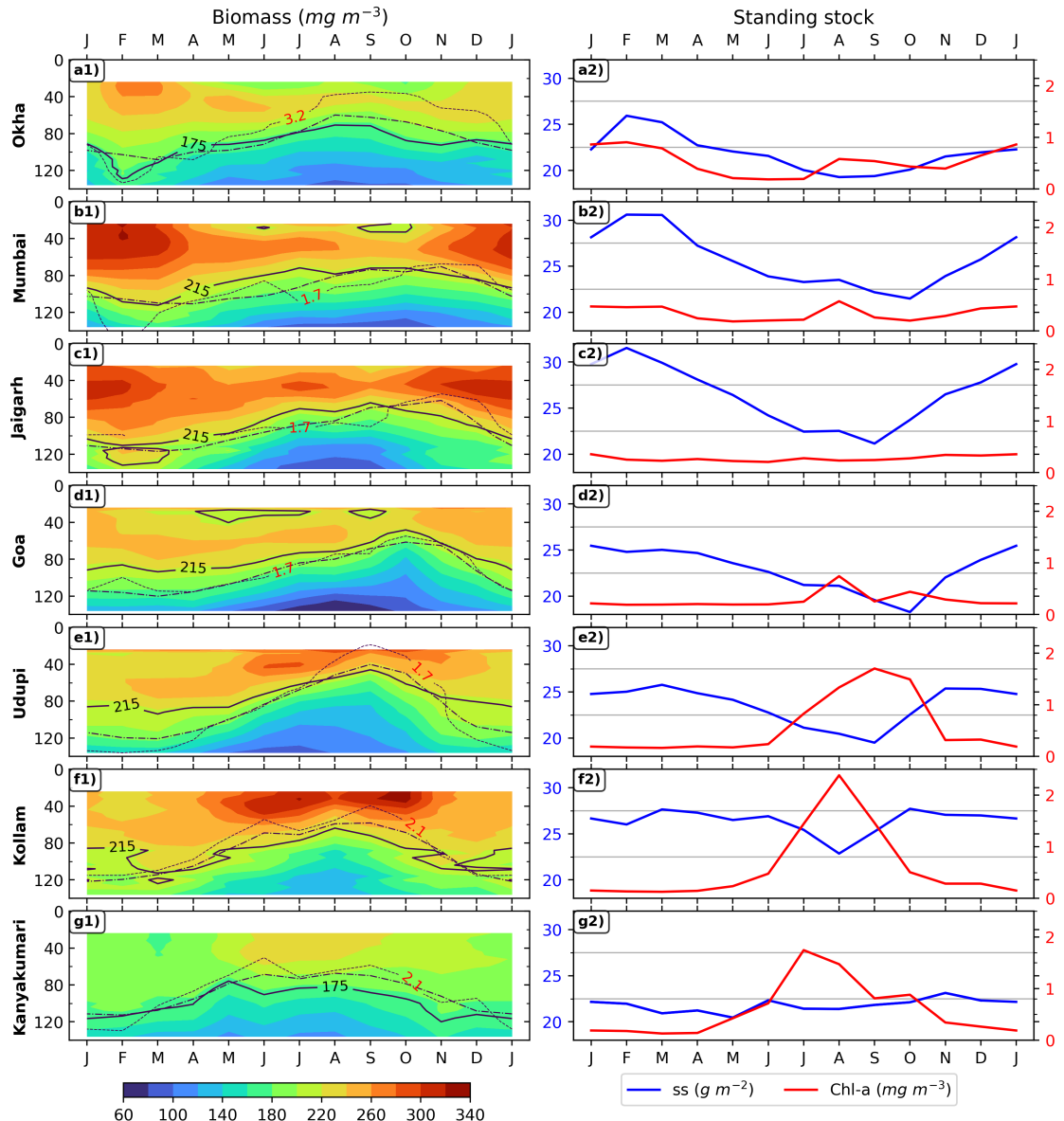


Figure 4: Monthly climatology of zooplankton biomass is shown in left panels for 7 locations, (top to bottom is southward). The D175 & D215 are shown in solid lines; dashed line represents the depth of 23 C isotherm; oxygen contours are shown in dotted lines and labeled for each mooring. The right set of panel plots is showing ZSS and chlorophyll climatology for corresponding locations.

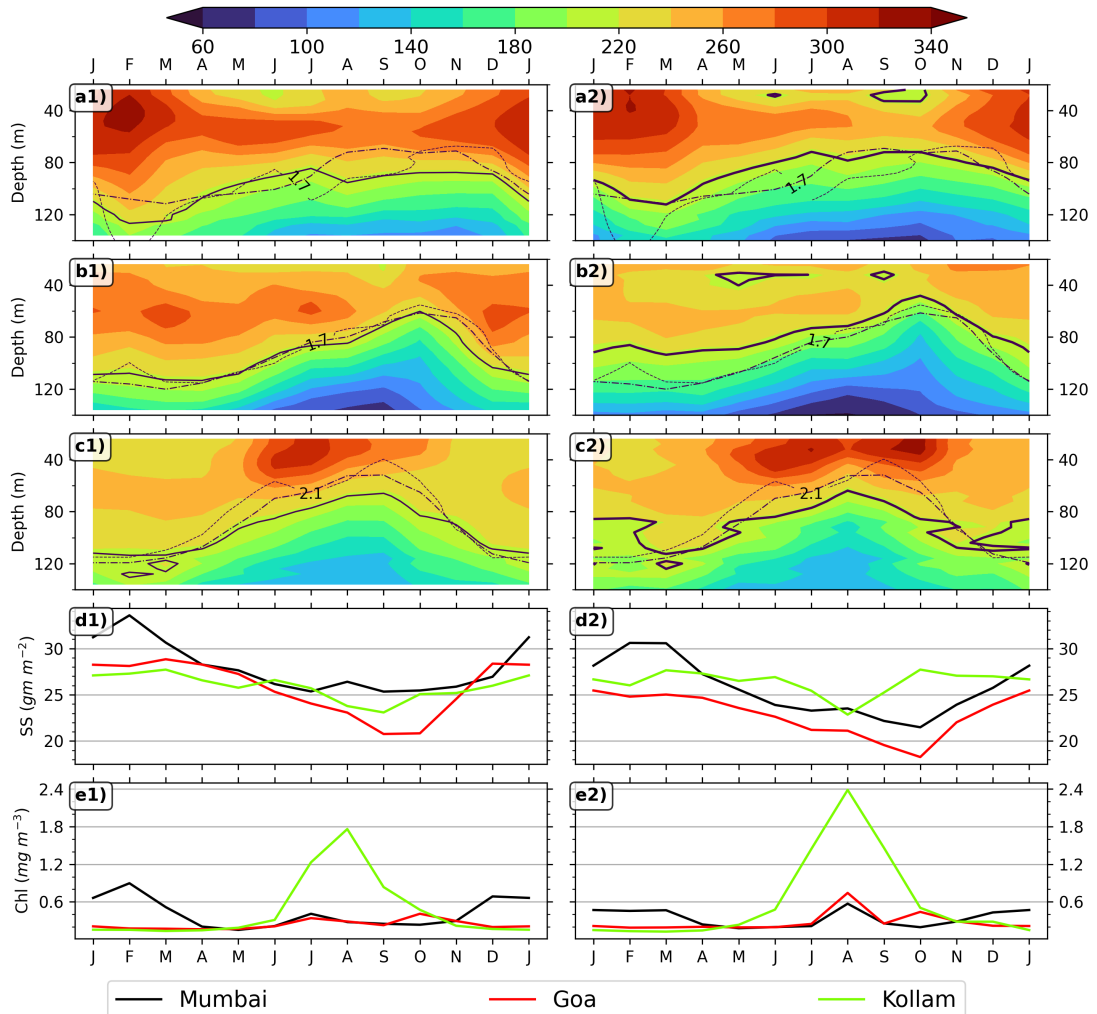


Figure 5: Monthly climatology of zooplankton biomass is shown in left panels for 3 locations which were earlier used in [Aparna et al., 2022]; a1, b1 & c1 is the biomass climatology for Mumbai, Goa and Kollam, d1 is for ZSS climatology, e1 is for chlorophyll biomass climatology; a2, b2, c2, d2 & e2 is same but based on data from 2017 to 2023. The D215 is shown in solid line. The dashed line represents the depth of 23 °C isotherm; oxygen contours are shown in dotted lines and labeled for each mooring.

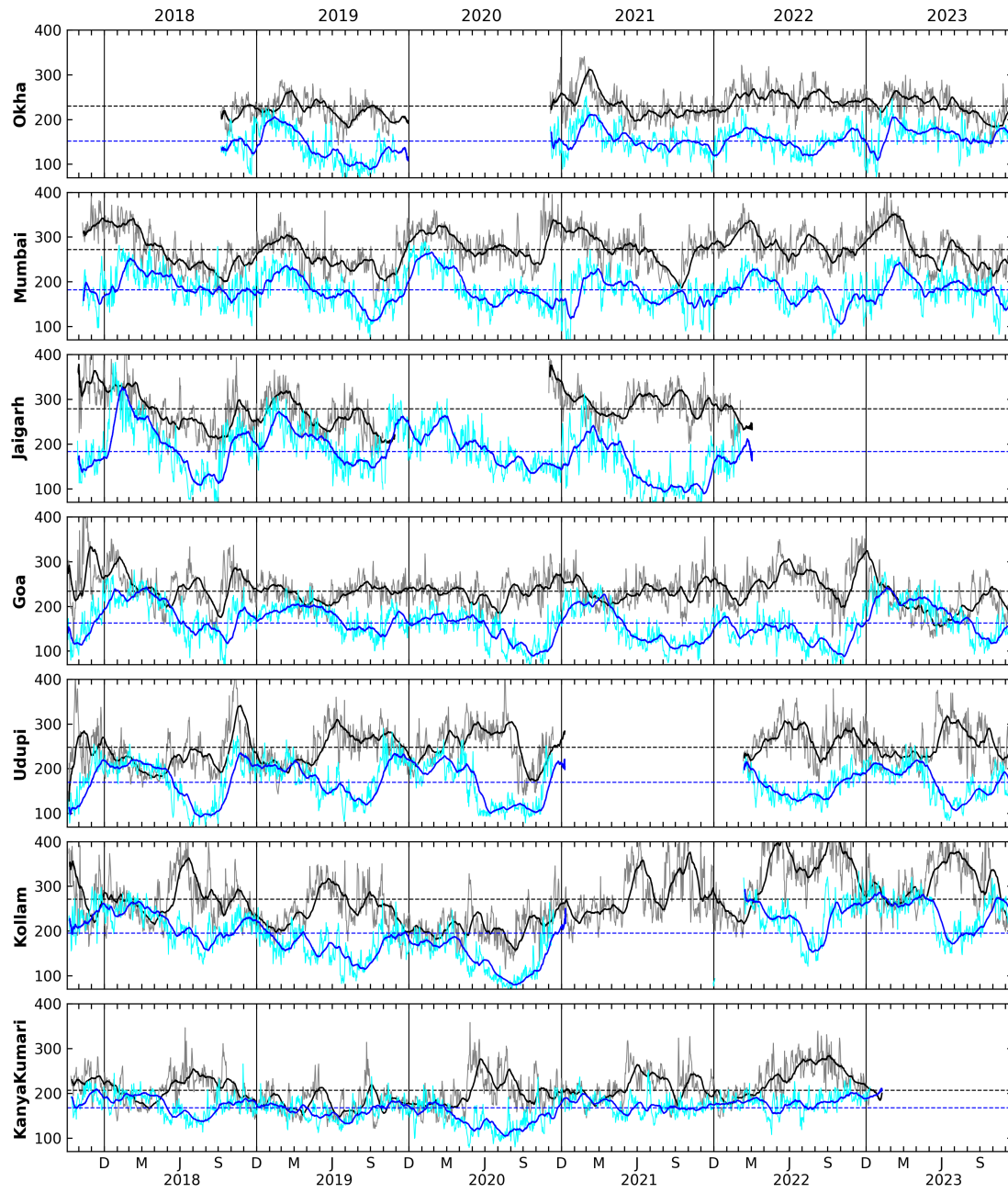


Figure 6: The daily biomass at depth of 40 m and 104 m for all locations shown by grey and cyan curves. The black and blue lines shows the 30 day rolling averaged biomass at 40 and 104 m, respectively. Notice the bursts seen in the daily data ranging from few days to weeks.

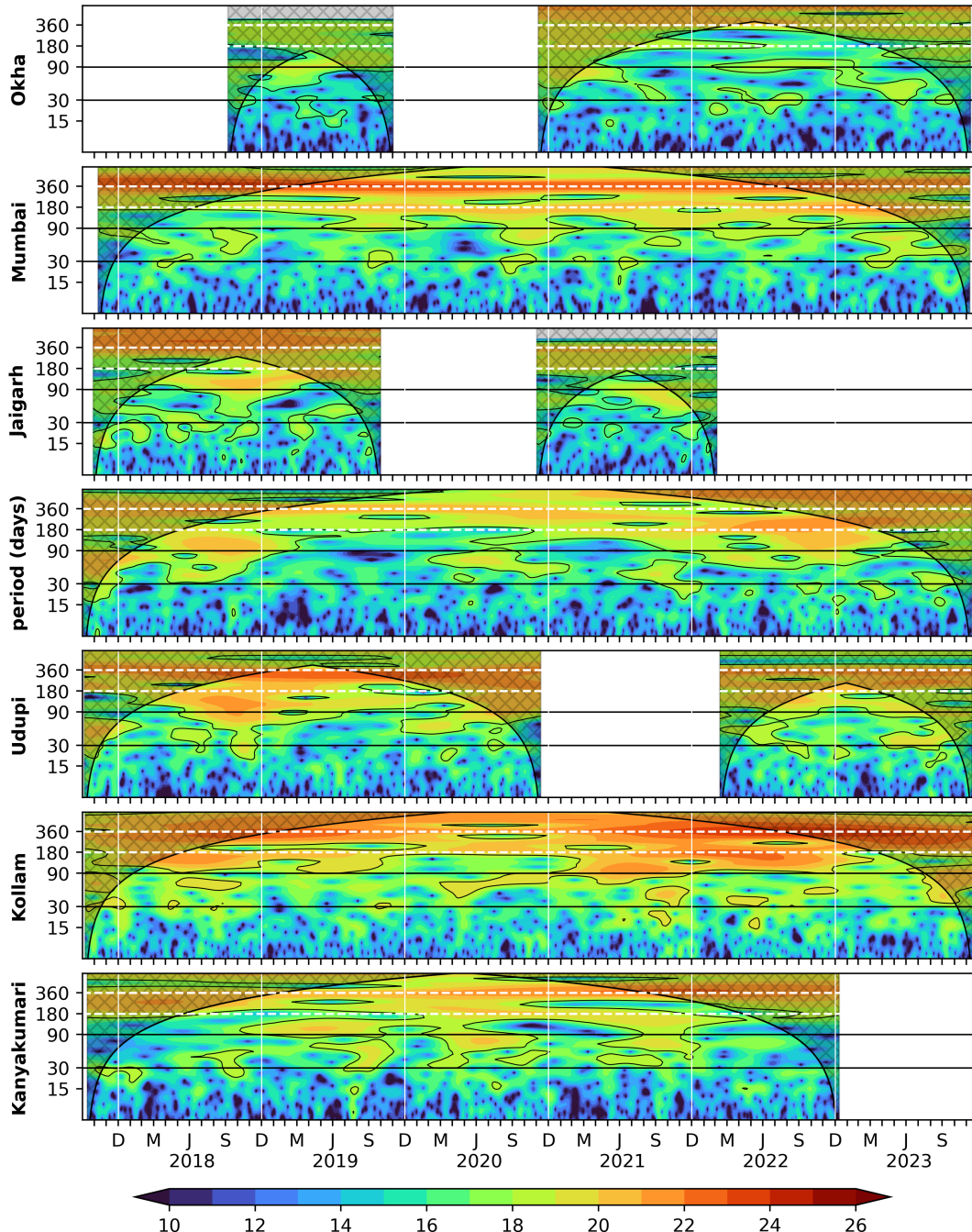


Figure 7: Wavelet power spectra (Morlet) of the 40 m zooplankton biomass plotted against time as abscissa and period in days as ordinate. The wavelet power is in \log_2 scale, the 95 % significance is marked in black contours; the cross-shaded region falls under cone of influence. Vertical white lines separates years.

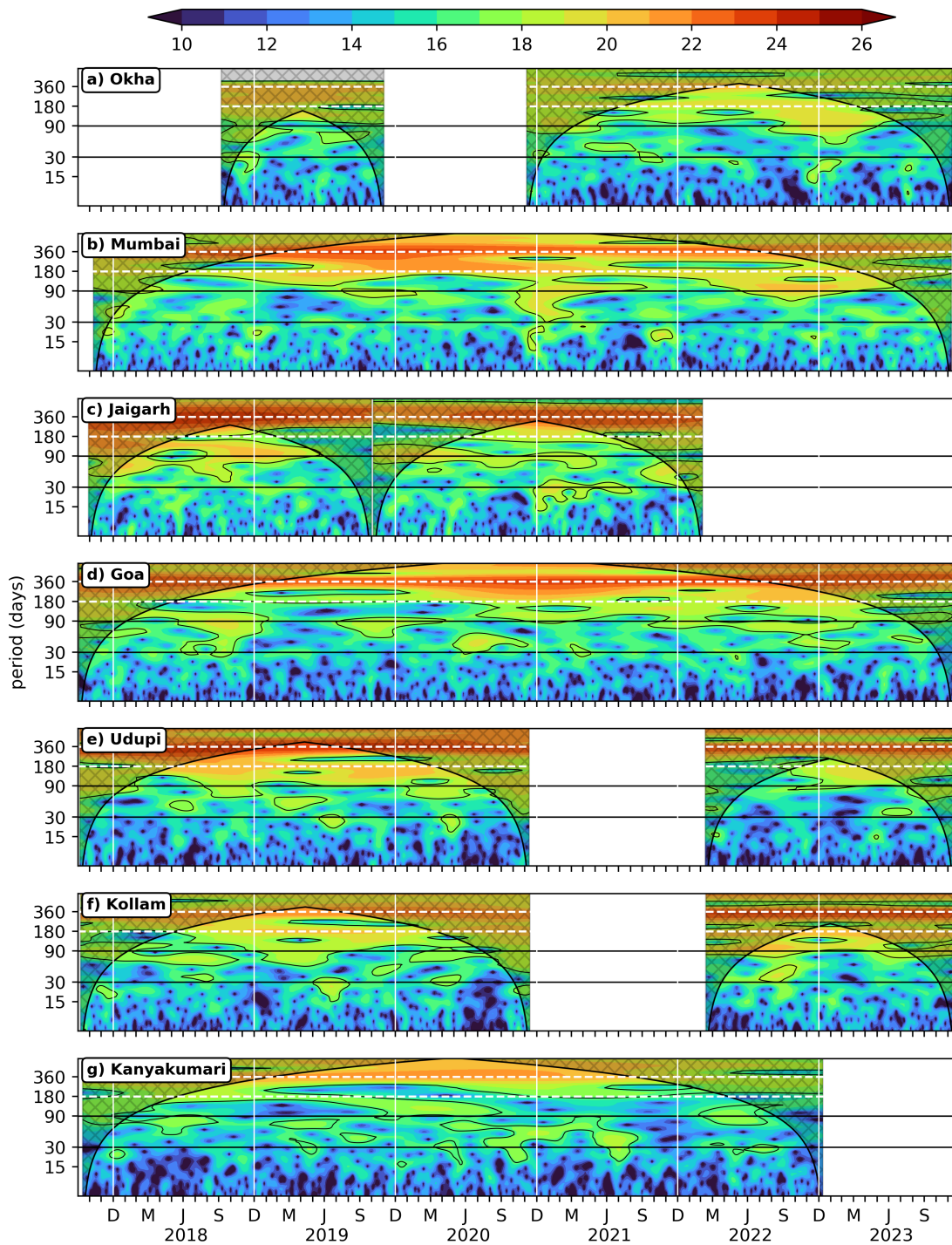


Figure 8: Wavelet power spectra (Morlet) of the 104 m zooplankton biomass plotted against time as abscissa and period in days as ordinate. The wavelet power is in log₂ scale, the 95 % significance is marked in black contours; the cross-shaded region falls under cone of influence. The vertical white lines separates years.

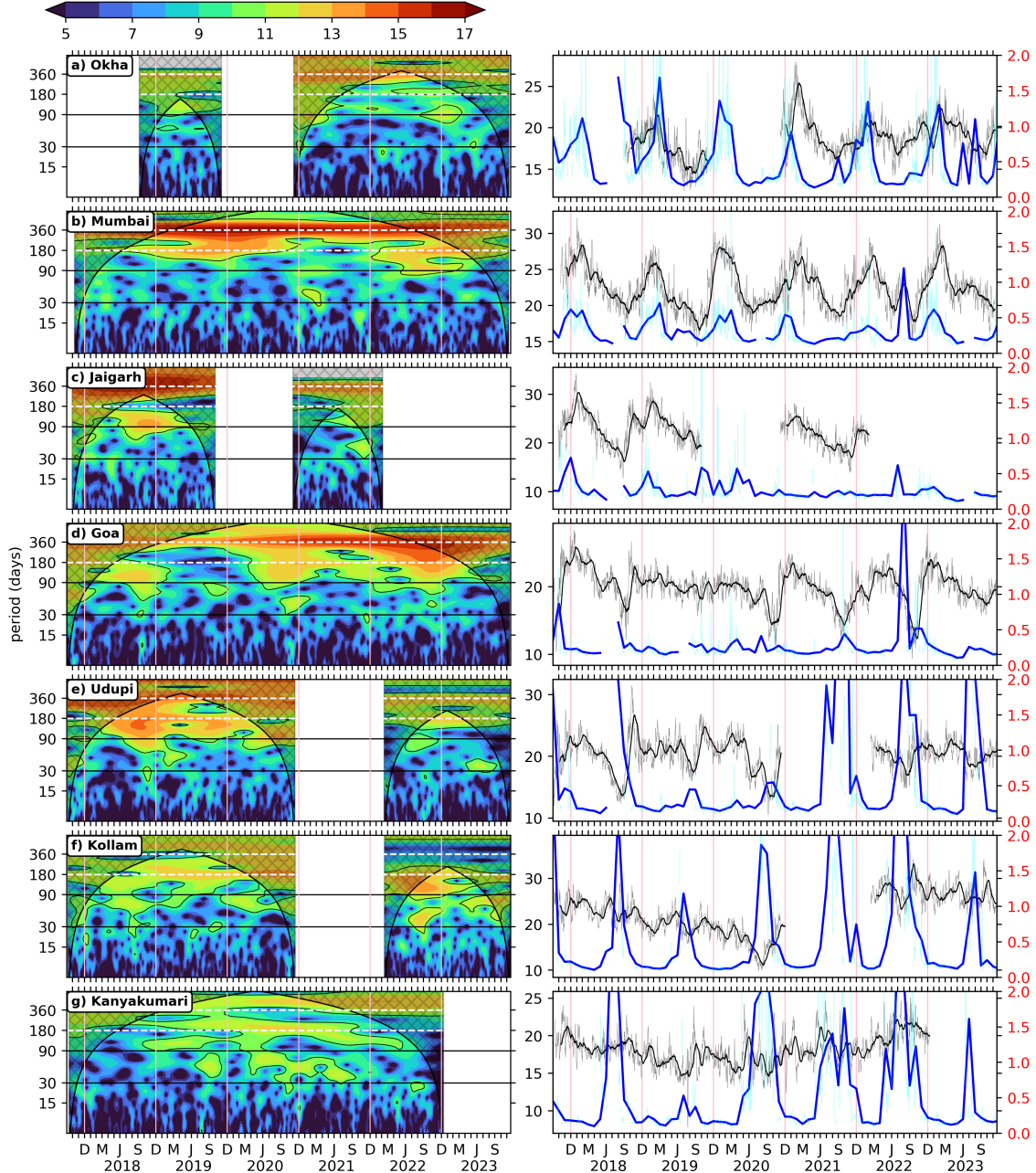


Figure 9: Wavelet power spectra (Morlet) of zooplankton standing stock plotted against time as abscissa and period in days as ordinate. The wavelet power is in log₂ scale, the 95 % significance is marked in black contours; The vertical white lines separates years. The right side panel shows the ZSS time series of 30 day rolling mean data (black)overlaid upon daily data (Grey). The 30 day rolling mean data of chlorophyll (solid blue line) is plotted over its daily data (cyan).

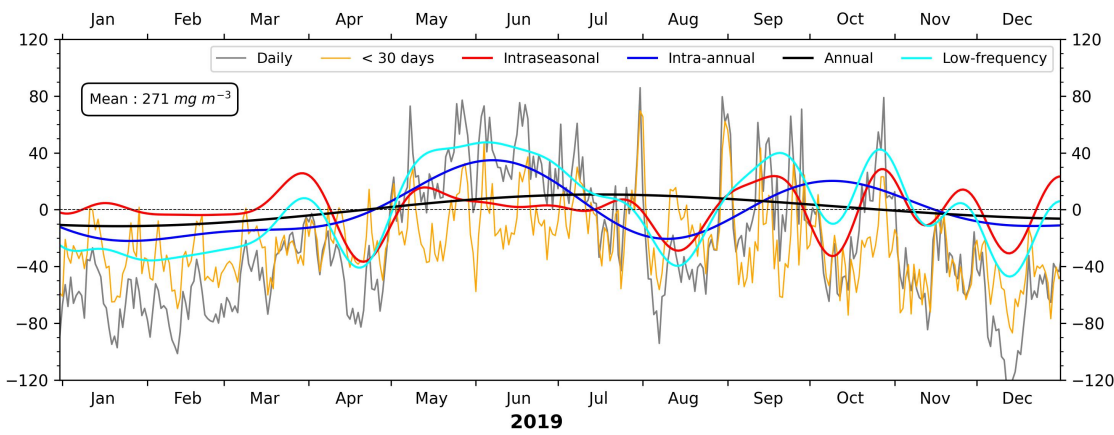


Figure 10: Comparison between mean-removed daily biomass time series at 40 m and the distinct components of variability off Kollam for 2019. The biomass units are mg m^{-3} . An increase in biomass is noticed from May onward and lasting till late monsoon with weeks of low biomass during August due to contribution from each component of variability. The cyan curve is sum of all low frequency components above 30 days, i.e, annual, intra-annual and 30 to 90 days intraseasonal variability.

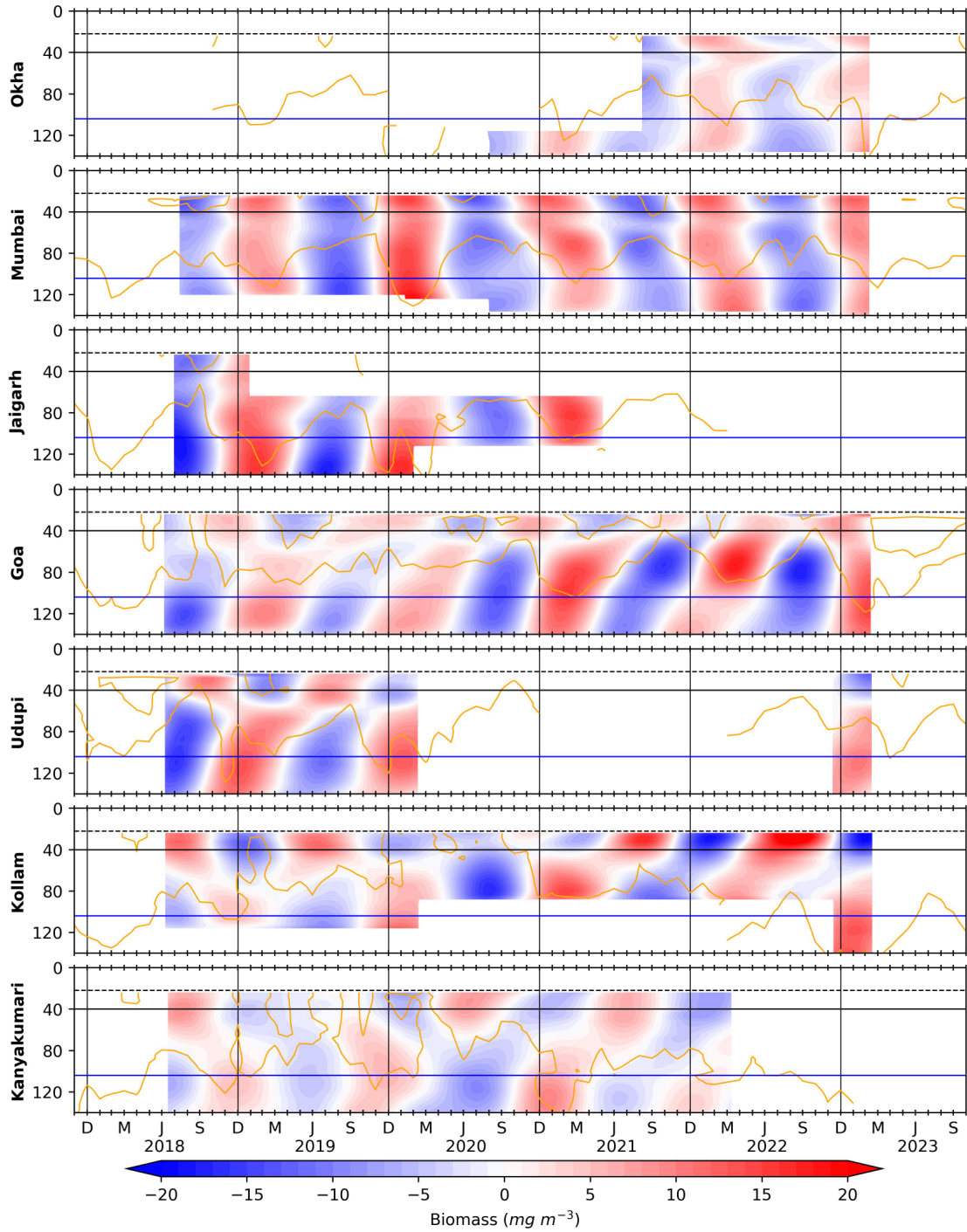


Figure 11: The biomass variation occurring in annual band (300 to 400 days). Owing to the presence of monsoon, there is a variation driven by associated upwelling (downwelling) processes in summer (winter) monsoon. and The horizontal black and blue lines is for 40 and 104 m respectively; vertical black lines separate the years. The dashed line at 22 m marks the top-depth of first bin i.e, 24 m ⁵² and solid orange curves denotes D215 (D175 off Okha and Kanyakumari)

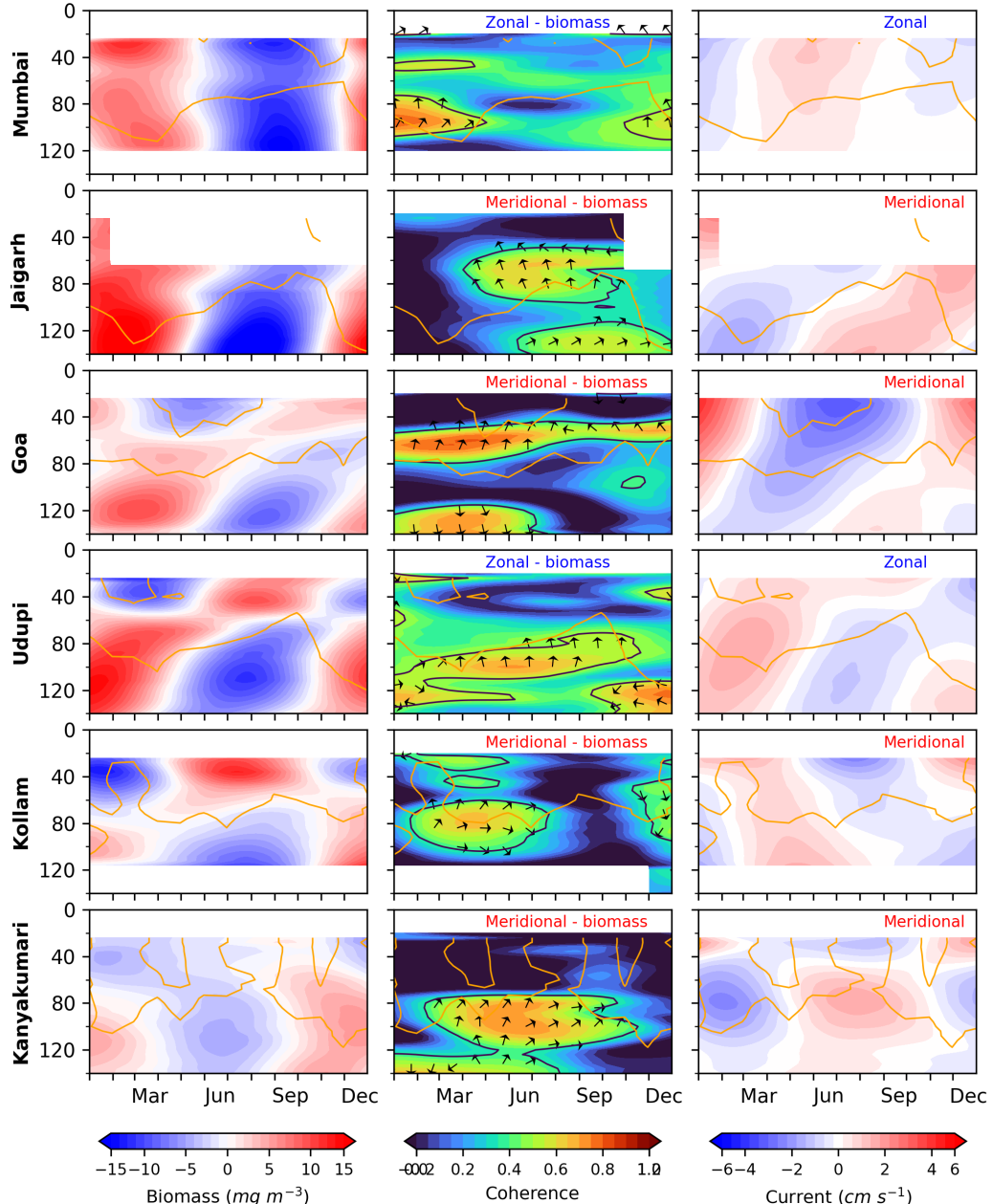


Figure 12: Current (zonal/meridional) and biomass wavelet coherence plotted alongside of annual filtered biomass and current. Either zonal or meridional current is considered depending on coherence and if current leads biomass. The solid contour encompasses greater than 0.5 coherence and phase is plotted with north as reference, +ve (-ve) x-axis is current leading (lagging) biomass. Left (Right) panel is for biomass (current). Although the annual biomass variability is weak and contributes less to the total biomass time series, upward phase propagation is seen implying upwelling favorable conditions leading to biomass growth. The solid orange curves denotes D215 (D175 off Okha and Kanyakumari)

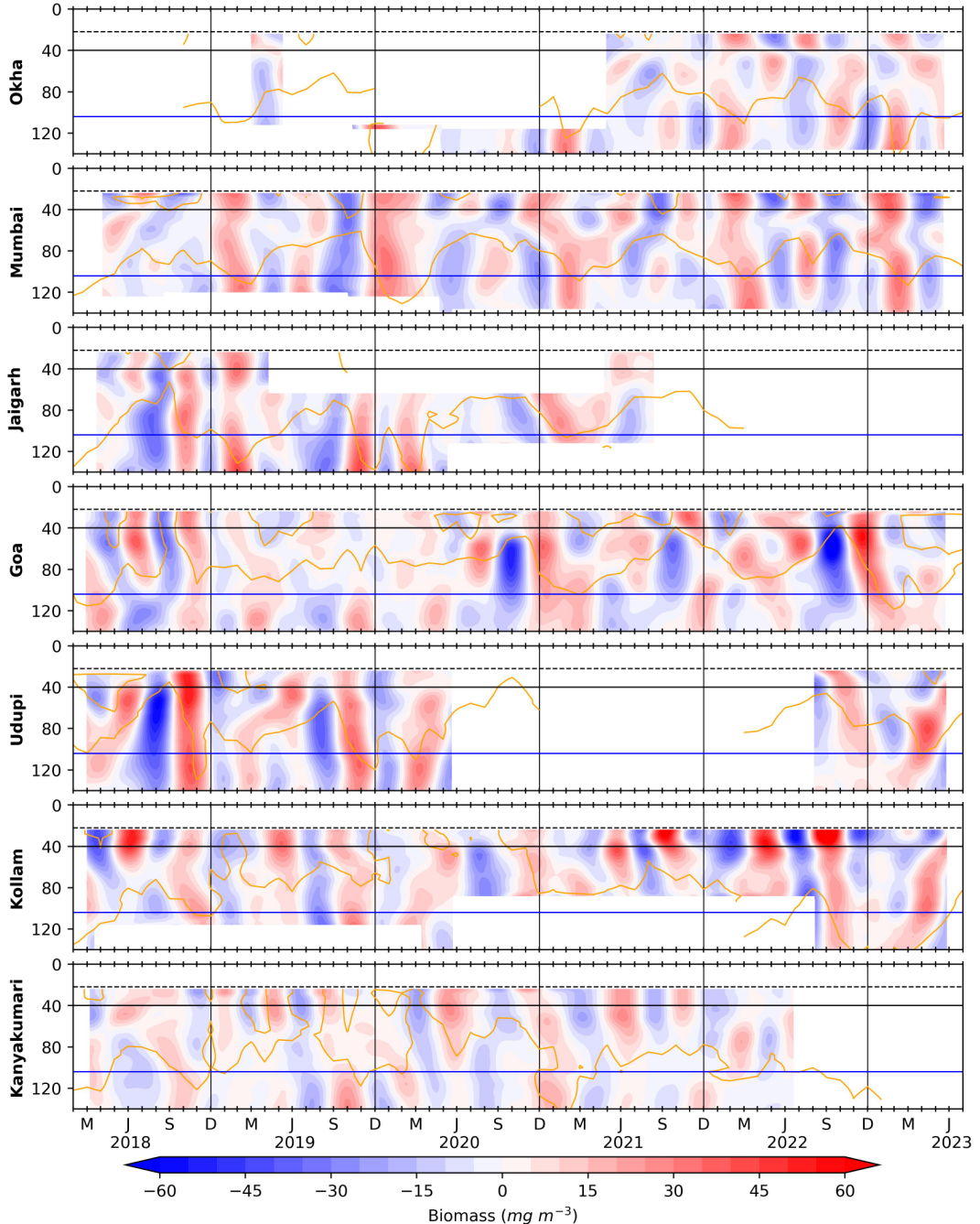


Figure 13: The biomass variation occurring in 100 to 250 days period (between the seasons and within a year record or intra-annual band) is obtained using a band pass filter. The horizontal black and blue lines is for 40 and 104 m respectively; vertical black lines separate the years. The dashed line at 22 m marks the top-depth of first bin i.e, 24 m and solid orange curves denotes D215 (D175 off Okha and Kanyakumari).

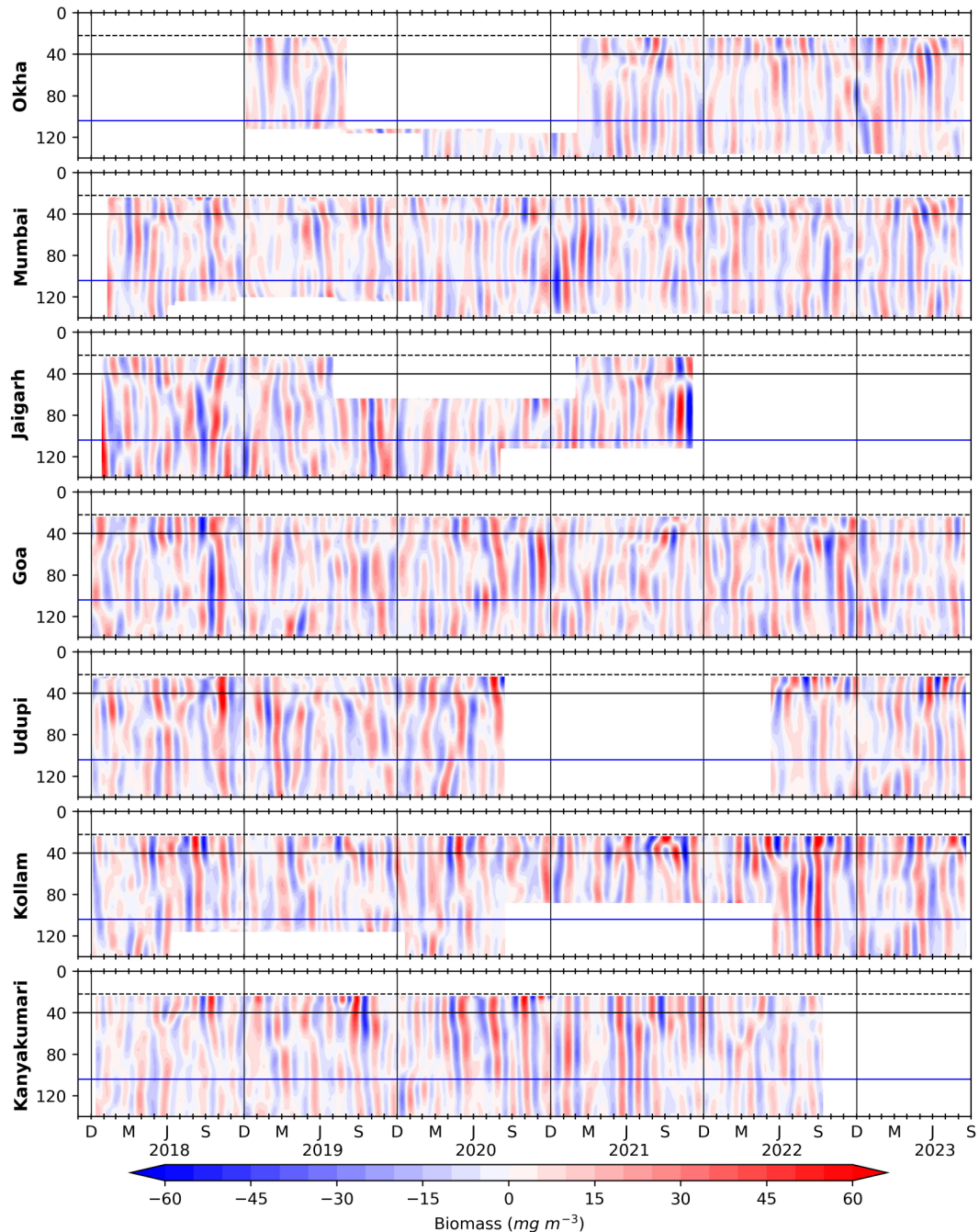


Figure 14: Biomass variation found in the scale of 30 to 90 days period (Intra-seasonal band as it is within a season) is obtained using a lanczos band pass filter. The horizontal black and blue lines is for 40 and 104 m respectively; vertical black lines separate the years. The dashed line at 22 m marks the top-depth of first bin i.e, 24 m. Intraseasonal variability is seen throughout the record and the variability is stronger during August to November.